Check for updates

Shannon and von Neumann entropies of multi-qubit Schrödinger's cat states†

Nathan D. Jansen, [ID] * Matthew Loucks, [ID] Scott Gilbert, [ID]
Corbin Fleming-Dittenber, [ID] Julia Egbert [ID] and Katharine L. C. Hunt [ID] *

Using IBM's publicly accessible quantum computers, we have analyzed the entropies of Schrödinger's cat states, which have the form $\Psi = (1/2)^{1/2} [|0\,0\,0\cdots0\rangle + |1\,1\,1\cdots1\rangle]$. We have obtained the average Shannon entropy S_{So} of the distribution over measurement outcomes from 75 runs of 8192 shots, for each of the numbers of entangled qubits, on each of the quantum computers tested. For the distribution over N fault-free measurements on pure cat states, S_{So} would approach one as N → ∞, independent of the number of qubits; but we have found that S_{So} varies nearly linearly with the number of qubits n. The slope of S_{So} *versus* the number of qubits differs among computers with the same quantum volumes. We have developed a two-parameter model that reproduces the near-linear dependence of the entropy on the number of qubits, based on the probabilities of observing the output 0 when a qubit is set to $|0\rangle$ and 1 when it is set to $|1\rangle$. The slope increases as the error rate increases. The slope provides a sensitive measure of the accuracy of a quantum computer, so it serves as a quickly determinable index of performance. We have used tomographic methods with error mitigation as described in the qiskit documentation to find the density matrix ρ and evaluate the von Neumann entropies of the cat states. From the reduced density matrices for individual qubits, we have calculated the entanglement entropies. The reduced density matrices represent mixed states with approximately 50/50 probabilities for states $|0\rangle$ and $|1\rangle$. The entanglement entropies are very close to one.

I. Introduction

We have evaluated the von Neumann entropy[1] and two forms of the Shannon entropy[2,3] for n-qubit Schrödinger's "cat" states[4] constructed on IBM's publicly accessible quantum computers.[5] In this work, we compare the empirical results with the predicted results for pure cat states and fault-free measurements. The qubits in the cat states are entangled, with wave functions of the form

$$\Psi = (1/2)^{1/2} [|0\,0\,0\cdots0\rangle + |1\,1\,1\cdots1\rangle], \qquad (1)$$

where $|0\,0\,0\cdots0\rangle$ denotes the tensor product of the state $|0\rangle$ for qubits $q[0]$ through $q[n-1]$, and similarly $|1\,1\,1\cdots1\rangle$ denotes the tensor product of the state $|1\rangle$ for $q[0]$ through $q[n-1]$.

The von Neumann entropy[1] S_{vN} is derived from the density matrix ρ. For the cat states, we cast S_{vN} in the form,

$$S_{vN} = -\mathrm{Tr}(\rho \log_2 \rho). \qquad (2)$$

Department of Chemistry, Michigan State University, East Lansing, Michigan,
48824, USA. E-mail: jansenn1@msu.edu, huntk@msu.edu

† Electronic supplementary information (ESI) available. See DOI: 10.1039/d1cp05255a

We have used the base-2 logarithm and omitted multiplication by the Boltzmann constant, because that allows for a more intuitive interpretation of the numerical value of S_{vN}. In eqn (2), Tr denotes the trace of the matrix that follows it, and the base-2 logarithm of the matrix ρ is the matrix r such that $2^r = \rho$. A pure cat state has a von Neumann entropy of zero.

By use of quantum state tomography[6–29] on the 5-qubit quantum computers ibmq_lima,[30] ibmq_manila,[31] and ibmq_belem,[32] we have found non-zero values of the von Neumann entropy for cat states with n = 2 to 5. The entropy is reduced by the error-mitigation method suggested in the qiskit documentation.[6] We have obtained the reduced density matrices for individual qubits by taking the partial traces of the density matrix over the remaining qubits.[33,34] In an entangled system, the reduced density matrix often characterizes a mixed state, even when the system as a whole is in a pure state.[35–44] The von Neumann entropy of a reduced density matrix for an individual qubit in an entangled state is termed the entanglement entropy.[35–44] We have found that the entanglement entropy comes very close to the ideal value of one, for each of the qubits in the cat states we have tested.

We have also used the density matrices to evaluate the Shannon entropy[2,3] S_{Sd} of the cat states as they reside on a quantum computer; S_{Sd} is determined by the probabilities p_j for

7666 | *Phys. Chem. Chem. Phys.*, 2022, **24**, 7666–7681

This journal is © the Owner Societies 2022

the quantum system to be found in each particular state $|j\rangle = |s_0 s_1 s_2 \cdots s_n\rangle$, where $s_k = |0\rangle$ or $|1\rangle$, and j runs from 1 to 2^n for an n-qubit state. The probability p_j is given by the jth diagonal element of the density matrix in the basis $\{|s_0 s_1 s_2 \cdots s_n\rangle\}$, and then S_{Sd} is obtained from[2,3]

$$S_{Sd} = -\sum_{j=1}^{2^n} p_j \log_2 p_j. \tag{3}$$

The Shannon entropy S_{Sd} for a pure cat state is one, independent of the number of entangled qubits, because the two components $|0\,0\,0\cdots0\rangle$ and $|1\,1\,1\cdots1\rangle$ are equally probable, and no other component contributes.

We have used eqn (3) to determine a second Shannon entropy S_{So}, which is defined as the average entropy of the distribution of measurement outcomes, based on multiple runs with 8192 shots. In computing the entropy in an individual run, we set p_j equal to the probability of the jth measurement outcome. When the wave function of a pure cat state collapses upon measurement, no outcomes other than $0\,0\,0\cdots0$ and $1\,1\,1\cdots1$ would be observed in the absence of measurement errors. Thus, the Shannon entropy S_{So} derived from N fault-free measurements of a pure cat state would approach one in the limit as $N \rightarrow \infty$, independent of the number of entangled qubits. If the measurement outcomes were entirely random, then p_j would equal $1/2^n$ for each j, and S_{So} would be equal to n.

We have obtained S_{So} from 75 runs of 8192 shots for each n value, up to the available number of qubits, on each of the IBM computers that were publicly accessible during this study.[5] The slope of S_{So} versus n should be zero, for fault-free measurements on pure cat states. Empirically we have found that S_{So} for the cat states increases nearly linearly with the number of qubits in the state, and we have obtained high values of R^2 for the linear fits.

We have developed a model for the entropy S_{So} as a function of the number of qubits, based on the probability a of observing an outcome of 0 when a qubit is prepared in state $|0\rangle$ and the probability b of observing an outcome of 1 when a qubit is prepared in state $|1\rangle$. This model predicts a near-linear dependence of the entropy on the number of qubits, as observed. In the model, the slope of S_{So} versus n is smaller when the accuracy is higher. From our measurements, the slope of S_{So} versus n is smaller for the more accurate quantum computers; it differs among computers with the same quantum volumes. Our results show that the slope provides a sensitive and quickly computable index of performance for the quantum computers.

The qubit states $|0\rangle$ and $|1\rangle$ on the publicly accessible IBM quantum computers are not the states of a spin-1/2 particle. Instead, these computers have superconducting transmon qubits based on Josephson junctions operated at a temperature of 15 mK.[45–49] Quantum gates induce transitions between the two lowest states $|0\rangle$ and $|1\rangle$, which are effectively isolated from the rest of the states by the anharmonicity of the circuit and the choice of the frequency of the gate pulses. These qubits respond to quantum gates for rotation and inversion and to the Hadamard gate[50–52] just as spin-1/2 particles would. They are coupled in the same way by the CNOT (CX)[50,51,53] and Toffoli gates,[50,51,54] so they are conveniently described with the spin-state terminology. Thus, the n-qubit cat states generalize the Bell state $(1/2)^{1/2}$ $[|\alpha_1 \alpha_2\rangle + |\beta_1 \beta_2\rangle]$ for two spin-1/2 particles[55,56] and the Greenberger, Horne, Zeilinger (GHZ) state $(1/2)^{1/2}$ $[|\alpha_1 \alpha_2 \alpha_3\rangle + |\beta_1 \beta_2 \beta_3\rangle]$ for three spin-1/2 particles.[4]

We have experimented with two different circuit algorithms to produce the cat states. When preparing the two different types of circuits, we have started by applying an H gate[50–52] to one qubit. In the "harpsichord" circuit, that qubit is linked directly via a CNOT gate[50,51,53] (also labeled as a CX gate[53]) to each of the remaining qubits. In the "stair-step" circuit, an H gate is applied to one qubit, that qubit is linked via a CNOT gate to a second qubit, the second qubit is linked via a CNOT gate to the next qubit, and sequential CNOT linkages between successive qubits continue until all of the qubits have been linked. The stair-step circuit typically transpiles with fewer gates than the harpsichord circuit, and the slopes of the linear fits tend to be lower for the stair-step. The stair-step and harpsichord circuits are identical for the 2-qubit Bell states.

While multiple studies of the von Neumann and Shannon entropies have been carried out for quantum systems, to our knowledge there has been no systematic investigation of the entropies of cat states, of the type reported here. Quantum Shannon theory, the von Neumann entropy, and entanglement have been reviewed in lectures notes by Preskill.[57] In earlier studies involving the Shannon entropy, Fai et al. have determined the Shannon entropy experimentally for polarons in quantum dots.[58,59] In one study, an external electric field was applied.[60] The Shannon entropy of the distribution over electronic states accompanying an S_N2 reaction has been modeled computationally.[61] Bera et al. have analyzed the relaxation dynamics of the Shannon entropy of dipolar bosons in a harmonic trap.[62]

Other entropy functions have been used to characterize quantum systems as well, most notably the Rényi entropy $S_R(q)$,[63–72] which is defined in terms of the density matrix by

$$S_R(q) = 1/(1-q)\log_2(\text{Tr}\,\rho^q). \tag{4}$$

The von Neumann, Shannon, and Rényi entropies are additive for independent systems. The Shannon entropy S_{So} generally differs from the standard thermodynamic entropy. But for a system in thermal equilibrium with p_j given by $\exp(-E_j/kT)/Q(N,V,T)$, in terms of the energy E_j of state j, the temperature T, the Boltzmann constant k, and the partition function $Q(N,V,T)$, $S_{So} = S_{vN}$ and the thermodynamic entropy is equal to S_{So} (or S_{vN}) multiplied by $k/\log_2 e$. The Rényi entropy $S_R(q)$ reduces to the Shannon entropy in the limit as $q \rightarrow 1$.[63]

The Wehrl information entropy[73,74] has been analyzed for cat states by Miranowicz et al.[75] The Tsallis entropy,[71,76,77] which is non-additive, has been applied in work on entanglement detection,[78] entanglement characterization,[79] and decoherence of qubits.[80,81] Brukner and Zeilinger have suggested a quadratic function of the probabilities of measurement outcomes as a new measure of information.[82,83] Based on studies of entropy production when a time-dependent external force acts on a spin system that is strongly coupled to a non-Markovian heat bath, Sakamoto and Tanimura[84] have suggested replacing the von

Neumann entropy with the entropy derived from Boltzmann's H theorem,[85] because Boltzmann's H function accounts explicitly for the entropy changes due to the system-bath interactions.[84]

Experimental measurements on entangled qubits and entangled photons have established the quantum mechanical behavior of Bell states, first with the work of Freedman and Clauser in 1972,[86] work by Fry and Thompson in 1976,[87] and then a series of studies in 1981 and 1982 by Aspect and co-workers,[88–90] who closed a number of the detection loopholes in their work on the violation of the Clauser–Horne–Shimony–Holt (CHSH) inequality.[91] Subsequent research has focused on closing coincidence-time, fair-sampling, detector efficiency, and "clumsiness" loopholes,[92–100] ensuring randomness of the measurement settings,[101,102] and demonstrating entanglement between widely separated photons.[103,104] The experiments show violations of the Bell[55,56] and CHSH inequalities[91] that rule out local hidden variable theories.[105] Violations of these inequalities, the related Mermin inequalities[106,107] and a Leggett–Garg inequality[108,109] have been demonstrated on quantum computers[110–112] (see also ref. 113 and 114). An entropic variant of the Bell inequalities is also violated quantum mechanically, though for different angles than the standard inequalities.[115] Chang et al. have formulated a multi-qubit variant of the Bell inequalities; they connected the maximal violation to the topological entanglement entropy.[116] Elben et al. have demonstrated a method of detecting entanglement in mixed states, based on local randomized measurements.[117]

In work on the preparation of cat states, Pan et al.[118] first reported the experimental preparation of a GHZ state for photons, and Lavoie, Kaltenbaek, and Resch[119] proved that a GHZ state exhibits nonlocality. Six-ion cat states that generalize the GHZ state have been prepared by Leibfried et al., using two hyperfine ground states of the beryllium ion as the individual-qubit basis states.[120] Wei et al. have verified multipartite entanglement of an 18-qubit GHZ state with an entanglement metric based on multiple quantum coherences; they found a fidelity of 0.5165 ± 0.0036.[121] Later, Mooney et al.[122] have generated and verified 27-qubit GHZ states with a fidelity of 0.546 ± 0.017 on the quantum computer ibmq_montreal[123] after quantum readout error mitigation, with a detectable improvement in fidelity after parity verification. The same investigators[124] have demonstrated entanglement of all 53 qubits on ibmq_rochester[125] and all 65 qubits on ibmq_manhattan.[126] Earlier, Sager, Smart, and Mazziotti[127] had prepared states interpretable as exciton condensates of photon particles and holes on ibmq_rochester, using 53 qubits. They proved that a condensate state had formed, because they found several eigenvalues larger than one, for the reduced particle–hole density matrix, modified to remove the ground state resolution. Their simulations showed the predicted result of 26.5 for the largest eigenvalue in the case of the 53-qubit condensate, though the eigenvalue obtained directly from the quantum computer was not as large.[127] The experimentally feasible formation of GHZ states with 2000 atoms in a high-finesse optical cavity via an entanglement amplification technique has been proposed by Zhao et al.[128]

As a counterpart to the GHZ state, Dür, Vidal, and Cirac[129] have identified the W state, which is given by $(1/3)^{1/2} [|\alpha(1) \alpha(2)$ $\beta(3)\rangle + |\alpha(1) \beta(2) \alpha(3)\rangle + |\beta(1) \alpha(2) \alpha(3)\rangle]$. The W state has been studied experimentally by Eibl et al.[130] Like the Bell and GHZ states, the W state shows non-classical behavior. In W states, entanglement persists even after particle loss.[131] Häffner et al. have prepared a generalized W state with up to eight ^{40}Ca$^+$ ions in a linear Paul trap; the qubit states were represented by the ^{2}S$_{1/2}$ ground state and a metastable ^{2}D$_{5/2}$ state.[131] Omran et al. have produced and manipulated cat states of the form $(1/2)^{1/2}$ $[|0\,1\,0\,1\cdots\rangle + |1\,0\,1\,0\cdots\rangle]$ in a one-dimensional array of ^{87}Rb atoms with up to twenty qubits.[132] They encoded qubit-state $|0\rangle$ with the ground state of the atom and encoded $|1\rangle$ with a Rydberg state.[132]

J. M. Deutsch and co-workers have used the entanglement entropy to investigate the development of statistical distributions within a subsystem of an entangled system in a pure state.[35,38,133] The rest of the system effectively acts as a bath for the smaller subsystem, allowing the distribution over the eigenstates of the subsystem to thermalize.[35,38,133] Then the entanglement entropy becomes equal to the thermodynamic entropy. Working with a Bose–Einstein condensate of ^{87}Rb atoms,[134,135] Greiner, Lukin, and co-workers have examined the development of thermal distributions of the occupancies of sites in an optical lattice, when the coupling between sites is changed abruptly.[41] Similar behavior has been observed for one fermion in an entangled multi-fermion system, with a sudden change in the Hamiltonian.[136–138] Localization due to disorder may prevent thermalization, however;[139] on the other hand, in many-body systems with power-law interactions, even when localization occurs, algebraic growth of entanglement entropy has been found.[140]

D. Deutsch has used the Shannon entropy S_{So} of the distribution over measurement outcomes to develop an alternate version of the uncertainty principle, with the goal of providing a fixed lower bound for the uncertainty.[141] His suggestion has been explored further by Jizba, Dunningham, and Joo,[142] Majernik and Opatrný,[143] Chen et al.,[144] and Veeren and de Melo.[145] Deutsch showed that if A and B are non-commuting operators for observables with sets of eigenvalues $\{a_i\}$ and $\{b_j\}$, then the sum of the distribution entropies $S_{SoA}(\{a_i\})$ and $S_{SoB}(\{b_j\})$ is bounded below,[141] although the greatest lower bound has not yet been identified. Bergh and Garttner have suggested the use of entropic uncertainty relations to detect entanglement.[146,147]

In Section II of the current work, we describe one construction of the Schrödinger's cat states and then present results for the von Neumann entropies of n-qubit states and the entanglement entropies of single qubits. In Section III, we present our results for the Shannon entropies S_{Sd} and S_{So}. We show that S_{So} is nearly linear in the number of qubits in the cat state. We describe a second circuit that we have used to construct the cat states and show how the slope of the near-linear relationship differs for the two circuits. The entropy depends on the number of gates used to implement the circuits, when transpiled. In Section IV, we present a simple model that yields a nearly linear relationship between the Shannon entropy S_{So} and the number of qubits n, based on the average probabilities of observing the values 0 and 1 upon measurement, when the qubits have been prepared in the states

7668 | Phys. Chem. Chem. Phys., 2022, **24**, 7666–7681

This journal is © the Owner Societies 2022

$|0\rangle$ and $|1\rangle$. In Section V, we discuss an algorithm-specific variant of the quantum volume[148–151] that applies to cat states, and we provide a brief summary. We conclude that the variation of the entropy with the number of qubits provides a useful index of performance for current quantum computers.

II. Circuit for Schrödinger's cat states, von Neumann entropy, and entanglement entropy

We have prepared the n-qubit Schrödinger's cat states on IBM's public quantum computers using qiskit. First, a Hadamard gate,[51] listed as h(q0), was applied to qubit $q[0]$. The remaining qubits were coupled sequentially *via* controlled-not (CNOT) gates,[51] so that $q[0]$ acts as the control for $q[1]$, then $q[1]$ acts as the control for $q[2]$, continuing until $q[n - 2]$ acts as the control for $q[n - 1]$. The CNOT gates are listed as cx[qi, qj] where qi is the control qubit and qj is the target. For example, the three-qubit cat states with $|\Psi\rangle = (1/2)^{1/2} (|0\,0\,0\rangle + |1\,1\,1\rangle)$ are coded as

$$h(q0)$$

$$cx([q0, q1], [q1, q2]),$$

corresponding to the stair-step algorithm.

We have determined the density matrices for the cat states using the code for entanglement verification provided in qiskit. Quantum tomography[6–29] relies on production and measurement of many states that are identical except for the effects of faults in their preparation. A GHZ state without transpilation or measurement is set up by get_ghz_layout; get_ghz_simple sets up a GHZ state with measurement. Both codes are included in Class BConfig, which parallelizes the CNOT gates to produce a circuit of less depth.[152] Theoretical state counts are determined from the ideal state vector produced by get_ghz_layout. For the actual GHZ states, tomography is carried out with state_tomography_circuits,[153] which requires 3^n circuits for an n-qubit state.[154] The codes in StateTomographyFitter[155] including fit[156] and state_fitter[157] apply the maximum likelihood method[158–161] to reconstruct the quantum state by convex optimization with CVXPY.[162,163]

Alternatives to the maximum likelihood method have been suggested, including a hedged maximum likelihood method,[164,165] a method involving an accuracy matrix,[166] maximization of the mean fidelity,[167] a method based on Bayesian inference,[168–170] and a maximal entropy approach that is well suited to reconstructing the density matrix when not all measurements can be performed with high fidelity.[28,171] Special considerations for the tomography of pure states have been described by Bagan *et al.*,[168] Jupp *et al.*,[172] and Gross *et al.*[173] The tomography of permutationally invariant states has been discussed by Tóth *et al.*[174] and by Moroder *et al.*[175]

The fidelity F of the density matrix is given by $F = [\text{Tr}(\rho_p^{1/2} \rho_T \rho_p^{1/2})^{1/2}]^2$, where ρ_p is the density matrix of the pure cat state, and ρ_T is the matrix found by tomographic experiments.[176] For the cat states, the fidelity is simply the sum of the four corner elements of the density matrix.[6] The fidelity may be improved by an error mitigation method that is included in the qiskit procedure for tomography. The raw density matrix is converted into a vector $\mathbf{v}_{\text{raw}}$, a calibration matrix $\mathbf{A}$ is constructed based on measurements, and then the error-mitigated density matrix $\mathbf{v}_{\text{cal}}$ in vectorized form is obtained by minimizing $||\mathbf{A}\mathbf{v}_{\text{cal}} - \mathbf{v}_{\text{raw}}||^2$ (ref. 177). The fitted density matrix may be constrained to be positive semi-definite.[177] The IBM documentation directs that tomography should not be performed on states with more than five qubits.

The computational time required for tomography grows exponentially with the number of qubits, because 3^n circuits are needed for quantum state tomography on an n-qubit cat state. We have examined the timing of runs with 2–5 entangled qubits on lima,[30] manila,[31] and belem.[32] The time is fit well as a function of the number of qubits n by the form $k_1\, 3^n + k_2$. The constant k_2 appears to reflect the overhead associated with the set-up time for the runs. Its inclusion improves the fit to the required times for 2- and 3-qubit cat states, but it is small compared with $k_1\, 3^n$ for the 4- and 5-qubit cat states. Further information and plots of the "time in system" are included in the ESI.†

As an example, the density matrix that we obtained for a 3-qubit GHZ state for a run on ibmq_santiago[178] is shown in Fig. 1. This density matrix is Hermitian, but not idempotent. We found the largest entries for the outer products $|0\,0\,0\rangle\langle0\,0\,0|$, $|0\,0\,0\rangle\langle1\,1\,1|$, $|1\,1\,1\rangle\langle0\,0\,0|$, and $|1\,1\,1\rangle\langle1\,1\,1|$, but additional coherences are present. The trace of the printed density matrix is 0.99998, reflecting rounding errors. The ratio of the sum of the two largest entries on the diagonal to the sum of the remaining entries on the diagonal is 9.7267. The trace of the square of the density matrix, which is an indicator of the purity of the state,[179,180] is 0.74926. The eigenvalues of the density matrix are 0.86210, 0.06038, 0.04157, 0.02152, 0.01442, −0.00001, 0.00000, and 0.00000; their sum is 0.99998, as expected. The negative eigenvalue almost certainly results from truncation error, based on the number of figures in the printed density matrix. For a pure quantum state, one of the eigenvalues of the density matrix is one, and the rest are zero.

The error-mitigated version of the density matrix ρ_m from the same run is also shown in Fig. 1. The trace of ρ_m is 1.00000. The ratio of the sum of the two largest entries on the diagonal to the sum of the other entries on the diagonal has been increased to 18.109 by the error mitigation procedure. Additional coherences are still present, as shown by the non-zero entries in the density matrix for outer products of non-identical states, in addition to $|0\,0\,0\rangle\langle1\,1\,1|$ and $|1\,1\,1\rangle\langle0\,0\,0|$. The trace of the square of the error-mitigated density matrix has risen to 0.86761. The eigenvalues of the error-mitigated density matrix ρ_m are 0.93033, 0.03690, 0.02626, 0.00650, 0.00001, −0.00001, −0.00001, and 0.00000, and the sum of the eigenvalues is 1.00000. Again, the negative eigenvalues result from truncation errors.

The von Neumann entropy of the density matrix is zero for a pure quantum state, but the observed value for the matrix ρ is 0.82720. The von Neumann entropy of the error-mitigated density matrix ρ_m drops to 0.45771. The apparent presence of

This journal is © the Owner Societies 2022

Phys. Chem. Chem. Phys., 2022, **24**, 7666–7681 | **7669**

$$\rho = \begin{bmatrix} 0.45312 & 0.00522-0.00884i & -0.00383-0.02964i & 0.01536-0.0112i & 0.00737-0.0052i & -0.00329-0.01362i & 0.00585-0.00499i & 0.40462+0.02955i \\ 0.00522+0.00884i & 0.01178 & 0.00118+0.00607i & 0.00011+0.00182i & -0.00138+0.005i & -0.00313-0.00057i & -0.0017+0.00858i & -0.0026+0.00024i \\ -0.00383+0.02964i & 0.00118-0.00607i & 0.01295 & -0.00226-0.00199i & -0.00316+0.00245i & -0.00189-0.00124i & 0.00439+0.00141i & -0.0003+0.0246i \\ 0.01536+0.0112i & 0.00011-0.00182i & -0.00226+0.00199i & 0.00973 & 0.00604-0.00429i & 0.00724-0.00226i & 0.00495-0.00587i & 0.00908+0.00142i \\ 0.00737+0.0052i & -0.00138-0.005i & -0.00316-0.00245i & 0.00604+0.00429i & 0.0097 & 0.00594+0.00083i & 0.00372-0.00086i & -0.00075+0.00658i \\ -0.00329+0.01362i & -0.00313+0.00057i & -0.00189+0.00124i & 0.00724+0.00226i & 0.00594-0.00083i & 0.02147 & -0.00171-0.01594i & 0.0006+0.00839i \\ 0.00585+0.00499i & -0.0017-0.00858i & 0.00439-0.00141i & 0.00495+0.00587i & 0.00372+0.00086i & -0.00171+0.01594i & 0.02759 & 0.0205-0.00392i \\ 0.40462-0.02955i & -0.0026-0.00024i & -0.0003-0.0246i & 0.00908-0.00142i & -0.00075-0.00658i & 0.0006-0.00839i & 0.0205+0.00392i & 0.45364 \end{bmatrix}$$

$$\rho_m = \begin{bmatrix} 0.4566 & 0.00524-0.00478i & -0.01184-0.02143i & 0.01353-0.00911i & 0.00206-0.00055i & -0.00263-0.01648i & 0.01017-0.00119i & 0.45198+0.0342i \\ 0.00524+0.00478i & 0.00785 & -0.00097+0.00328i & -0.00139+0.00011i & -0.00194+0.00324i & -0.00383-0.00069i & -0.00286+0.00851i & -0.00266+0.00388i \\ -0.01184+0.02143i & -0.00097-0.00328i & 0.00845 & -0.00277+0.00012i & -0.00189+0.00079i & -0.00105+0.00035i & 0.00437+0.00276i & -0.00186+0.02538i \\ 0.01353+0.00911i & -0.00139-0.00011i & -0.00277-0.00012i & 0.00434 & 0.00196-0.00199i & 0.0041+0.00138i & 0.00192-0.00544i & 0.00621+0.00952i \\ 0.00206+0.00055i & -0.00194-0.00324i & -0.00189-0.00079i & 0.00196+0.00199i & 0.00478 & 0.0014+0.00254i & 0.00381-0.00046i & -0.00298+0.00442i \\ -0.00263+0.01648i & -0.00383+0.00069i & -0.00105-0.00035i & 0.0041-0.00138i & 0.0014-0.00254i & 0.00694 & -0.00129-0.00945i & -0.00987+0.01774i \\ 0.01017+0.00119i & -0.00286-0.00851i & 0.00437-0.00276i & 0.00192+0.00544i & 0.00381+0.00046i & -0.00129+0.00945i & 0.01997 & 0.0185-0.00079i \\ 0.45198-0.0342i & -0.00266-0.00388i & -0.00186-0.02538i & 0.00621-0.00952i & -0.00298-0.00442i & -0.00987-0.01774i & 0.0185+0.00079i & 0.49107 \end{bmatrix}$$

$$\rho_A = \begin{bmatrix} 0.50337 & 0.0294-0.01392i \\ 0.0294+0.01392i & 0.49663 \end{bmatrix}$$

$$\rho_B = \begin{bmatrix} 0.49608 & 0.0006-0.02029i \\ 0.0006+0.02029i & 0.50392 \end{bmatrix}$$

$$\rho_C = \begin{bmatrix} 0.48759 & 0.01771-0.00295i \\ 0.01771+0.00295i & 0.51241 \end{bmatrix}$$

Fig. 1 Density matrix ρ, error-mitigated density matrix ρ_m and reduced density matrices ρ_A, ρ_B, and ρ_C from one run for a GHZ state on santiago.[178] The basis for density matrices ρ and ρ_m is $\{|0\,0\,0\rangle, |0\,0\,1\rangle, |0\,1\,0\rangle, |0\,1\,1\rangle, |1\,0\,0\rangle, |1\,0\,1\rangle, |1\,1\,0\rangle, |1\,1\,1\rangle\}$. The basis for the reduced density matrices is $\{|0\rangle, |1\rangle\}$.

negative eigenvalues is not reflected in the value of the von Neumann entropy S_{vN} found with the qiskit procedure, since the negative eigenvalues would otherwise lead to an imaginary component of S_{vN}.

Reduced density matrices for individual qubits are obtained by taking a partial trace over the states of the remaining entangled qubits.[33,34] Labeling the first qubit as A and taking I_A as the identity operator for that qubit, labeling the two remaining qubits as B and C, and using $\otimes$ to denote a tensor product, the partial trace over B and C for a three-qubit density matrix ρ_T is given by

$$\rho_A = (I_A \otimes \langle \alpha_B \alpha_C|) \rho_T (I_A \otimes |\alpha_B \alpha_C\rangle) + (I_A \otimes \langle \alpha_B \beta_C|) \rho_T (I_A \otimes |\alpha_B \beta_C\rangle)$$
$$+ (I_A \otimes \langle \beta_B \alpha_C|) \rho_T (I_A \otimes |\beta_B \alpha_C\rangle) + (I_A \otimes \langle \beta_B \beta_C|) \rho_T (I_A \otimes |\beta_B \beta_C\rangle). \quad (5)$$

For pure cat states, the reduced density matrices represent mixed states, with vanishing coherences. The reduced density matrices for qubits A, B, and C (corresponding to $q[0]$, $q[1]$, and $q[2]$) are shown in Fig. 1. These density matrices are also Hermitian, with a trace of 1.00000 in each case. They represent mixed states with nonzero coherences. The trace of ρ_A^2 is 0.50214, the trace of ρ_B^2 is 0.50085, and the trace of ρ_C^2 is 0.50095. The traces of the squares of the error-mitigated reduced density matrices ρ_{Am}^2, ρ_{Bm}^2, and ρ_{Cm}^2 are similar. For a pure cat state, the traces of all of the ρ^2 values for individual qubits would be 0.5.

The von Neumann entropies of the reduced density matrices are all very close to one. For ρ_A, the von Neumann entropy is 0.99691; for ρ_B, the entropy is 0.99877; and for ρ_C, the entropy is 0.99863. The entropies of the error-mitigated reduced density matrices formed from the error-mitigated multi-qubit density matrix are not appreciably closer to one and may in fact be smaller. For ρ_{Am}, the von Neumann entropy is 0.99823; for ρ_{Bm}, the entropy is 0.99724; and for ρ_{Cm}, the entropy is 0.99793. For a mixed state with two possible measurement outcomes—0 or 1 for a single qubit—and no coherences, the von Neumann entropy would equal one if the two outcomes were equally probable. If the probabilities are not equal, the von Neumann entropy is given by

$$\begin{aligned} S_{vN} &= -(1/2+x)\log_2(1/2+x) - (1/2-x)\log_2(1/2-x) \\ &= 1 - (1/2+x)\log_2(1+2x) - (1/2-x)\log_2(1-2x) \\ &= 1 - \log_2(1-4x^2)^{1/2} - \log_2[(1+2x)/(1-2x)]^x, \end{aligned} \quad (6)$$

which applies in the current case. We note that Anaya-Contreras et al. have proposed a method to calculate the von Neumann entropy of a larger system from the entropy of a subsystem that is initially in a mixed state.[181]

In Table 1, we list the averages of five results for the von Neumann entropies of cat states coded with the stair-step algorithm, for numbers of qubits from 2 to 5. We also list the average Shannon entropies S_{Sd} derived from diagonal elements of the density matrices. Both the raw values and the error-mitigated values of S_{vN} and S_{Sd} are listed, along with the raw fidelities.

Table 1 The calculated von Neumann entropies S_{vN} of cat states with qubit numbers n from 2 to 5, the von Neumann entropies $S_{vN,m}$ after error mitigation, the Shannon entropies S_{Sd} derived from the diagonal elements of the density matrices, the Shannon entropies $S_{Sd,m}$ after error mitigation, and the raw fidelities F. The averages of five values from runs on lima,[30] manila,[31] and belem[32] are listed along with the standard deviations

	S_{vN}	$S_{vN,m}$	S_{Sd}	$S_{Sd,m}$	F
lima					
2	0.4176 ± 0.0281	0.1293 ± 0.0223	1.2703 ± 0.0254	1.1177 ± 0.0385	0.9255 ± 0.0031
3	0.6592 ± 0.0140	0.2313 ± 0.0297	1.4828 ± 0.0174	1.2139 ± 0.0166	0.8850 ± 0.0032
4	1.0558 ± 0.0247	0.2664 ± 0.0336	1.8558 ± 0.0112	1.3312 ± 0.0208	0.7989 ± 0.0062
5	1.5143 ± 0.0411	0.4003 ± 0.0664	2.2828 ± 0.0271	1.4981 ± 0.0539	0.6468 ± 0.0045
manila					
2	0.4300 ± 0.0381	0.0788 ± 0.0216	1.2411 ± 0.0104	1.0588 ± 0.0129	0.9286 ± 0.0048
3	0.8575 ± 0.0246	0.2200 ± 0.0367	1.5838 ± 0.0160	1.2093 ± 0.0324	0.8530 ± 0.0059
4	1.2552 ± 0.0192	0.4684 ± 0.0356	1.9277 ± 0.0129	1.4163 ± 0.0266	0.7792 ± 0.0061
5	1.5823 ± 0.0357	0.7166 ± 0.0476	2.2249 ± 0.0266	1.6021 ± 0.0240	0.6785 ± 0.0116
belem					
2	0.7032 ± 0.0391	0.5278 ± 0.0516	1.3925 ± 0.0281	1.2902 ± 0.0333	0.8471 ± 0.0098
3	1.0247 ± 0.0341	0.6848 ± 0.0422	1.7013 ± 0.0144	1.4886 ± 0.0134	0.7909 ± 0.0072
4	1.4081 ± 0.0199	0.6810 ± 0.0407	2.1023 ± 0.0204	1.6454 ± 0.0483	0.7240 ± 0.0070
5	1.9810 ± 0.3303	0.9224 ± 0.3237	2.6981 ± 0.3363	1.8533 ± 0.1817	0.4977 ± 0.1668

The difference between the average values and the expected results for a pure cat state increases and the fidelity drops off as the number of qubits increases, monotonically in all cases. The standard deviations are also listed in Table 1. The results were obtained from runs on lima,[30] manila,[31] and belem.[32] We have observed appreciable variability in the von Neumann entropies from runs at different times, particularly for the 5-qubit cat states on belem.

III. Shannon entropies S_{Sd} and S_{So} for Schrödinger's cat states
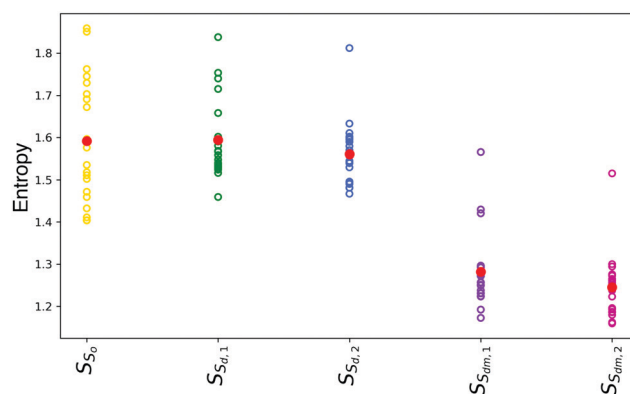
We have derived the Shannon entropies S_{Sd} of the cat states as they are resident in the computer by determining the density matrix in the basis $\{|j\rangle = |s_0 s_1 s_2 \cdots s_n\rangle\}$ by quantum state tomography.[6–29] We have used eqn (3), with p_j equal to the diagonal element of the density matrix for the state $|j\rangle$. If the density matrix were diagonal in the basis $\{|j\rangle = |s_0 s_1 s_2 \cdots s_n\rangle\}$, then S_{vN} and S_{Sd} would be identical; but since the basis states $|j\rangle$ are not the eigenstates of the density matrix, $S_{vN} \neq S_{Sd}$.

For the 3-qubit GHZ state taken as an example in Fig. 1, $S_{Sd} = 1.5833$. The Shannon entropy derived from the error-mitigated density matrix is denoted by $S_{Sd,m}$ and its value is 1.3668. Both are larger than the value of 1 expected for a pure cat state. In contrast, the Shannon entropies S_{Sd} of the reduced density matrices are all very close to their ideal value of 1: $S_{Sd,A} = 0.99997$, $S_{Sd,B} = 0.99996$, and $S_{Sd,C} = 0.99956$. The connection of the Shannon entropy to tomography has also been discussed by Chernega et al.[14]

Fig. 2 shows the spread of raw and error-mitigated values of S_{Sd} for two sets of twenty runs on 3-qubit cat states on jakarta[182] with 1024 shots per circuit, along with twenty values of S_{So} also obtained from runs on jakarta[182] with 1024 shots per job. The average value of S_{So} differs relatively little from the average of the raw values of S_{Sd} obtained from the two sets of runs, although the spread of S_{So} is somewhat greater. As expected, the error mitigation procedure reduces S_{Sd} noticeably, with a few outliers. We have found that the imaginary parts of the

entries for $|0\,0\,0\rangle\langle1\,1\,1|$ and $|1\,1\,1\rangle\langle0\,0\,0|$ in the raw density matrices are relatively large ($\sim$12–14% of the largest entries on the diagonal), and the imaginary parts are increased by the error mitigation procedure.

Direct calculations of S_{So}, which is defined as the average Shannon entropy of the distribution over measurement outcomes, require appreciably less time than the tomography to find S_{vN} and S_{Sd}. As a result, we were able to obtain a more extensive set of results for S_{So} from multiple quantum computers. We generated cat states in individual jobs, each consisting of 75 circuits with 8192 shots (the maximum number of circuits per job when this work was carried out, and the maximum number of shots per circuit). All of these jobs were executed on the quantum computers within the same calibration period, to ensure consistency between runs. Each circuit was tested on the simulator_statevector[183] to confirm that the circuit was interpreted as the intended fully entangled state. The simulator_statevector was used to confirm that S_{So} is very close to one for fault-free n-qubit cat states.

Fig. 2 The Shannon entropies S_{So} obtained from the distribution of measurement outcomes for individual runs and the Shannon entropies S_{Sd} derived from the diagonal elements of the density matrix, obtained via tomography for 3-qubit cat states on jakarta.[182] The Shannon entropies S_{Sdm} have been derived from the density matrices after error mitigation with routines from IBM's qiskit documentation.[6] Points in red indicate the averages of the results.

Deviations from $S_{So} = 1$ for the cat states on the simulator result from random statistical effects that cause the measurement outcomes $0\,0\cdots 0$ and $1\,1\cdots 1$ to differ slightly in number, reducing S_{So}.

In the executed versions of the code, the transpiler selected the activated qubits, so that the H gate was sometimes applied to qubits other than $q[0]$, though the overall coupling scheme was maintained. The transpiled Hadamard gate[51] was implemented by three operations, RZ SX RZ, where RZ is a rotation by $\pi/2$ around the Z axis and SX is the square-root of the Pauli spin matrix σ_X.[51] The operation RZ is accomplished by a change of basis, without the application of a pulse. The combination RZ SX RZ differs from the H gate by a phase, but the results of measurements are unaffected by the phase difference. The CNOT gates[51] were typically applied directly to qubits that were adjacent in the architecture of a particular quantum computer. If qubits qi and qj were not adjacent, however, the transpiler implemented a sequence of CNOT gates to accomplish the coupling between qi and qj as designated in the input circuit.

As an alternative to the stair-step circuits described in Section II, we also coded harpsichord circuits, in which each of the qubits after $q[0]$ is coupled back to $q[0]$ *via* CNOT gates. Thus $q[0]$ acts as the control qubit for all of the others. We have found that the transpilation of the harpsichord circuits is not unique. Fig. 3 shows the circuit diagram after transpilation of the stair-step algorithm and three different circuit diagrams for the harpsichord algorithm, for 4-qubit cat-states on manila.[31]

The entropy S_{So} for each set of outcomes with 8192 shots was calculated using eqn (3). Table 2 shows the entropy values averaged over the 75 circuits in each job. The averages are listed for each of the computers, each of the numbers of entangled qubits n, and the two coupling algorithms. In Fig. 4, the entropy S_{So} is plotted *versus* the number of qubits n for the stair-step algorithm run on ibmq_yorktown,[184] ibmq_belem,[32] ibmq_manila,[31] ibmq_athens,[185] and ibmq_santiago,[178] with n from 2 to 5. In Fig. 5, S_{So} is plotted *versus* n for the stair-step algorithm and the harpsichord algorithm on yorktown, athens, and santiago, to illustrate the difference between the entropies found with the two different algorithms. For both algorithms on all of the quantum computers we used, we have found nearly linear relationships between S_{So} and the number of qubits n. The dashed lines in Fig. 4 and 5 show the least-squares fits of straight lines to the results, weighted by the inverses of the variances.

Table 3 shows the linear least-squares fits and the coefficients of determination (the R^2 values) for each fit, for ibmq_santiago,[178] ibmq_athens,[185] ibmq_manila,[31] ibmq_belem,[32] ibmq_lima,[30] ibmq_quito,[186] ibmq_yorktown,[184] and ibmq_melbourne.[187] In the fitting procedure, the data have been weighted by the inverses of the variances. The fit of S_{So} *versus* n to a straight line is good in all cases, with R^2 values ranging from 0.9617 to 0.9998. For perfectly constructed cat states with no measurement errors, the slopes would be zero. A smaller value of the slope indicates better performance of the quantum computer. We have found the smallest slope for the stair-step algorithm on santiago ($m = 0.1565$, $R^2 = 0.9746$), and the largest
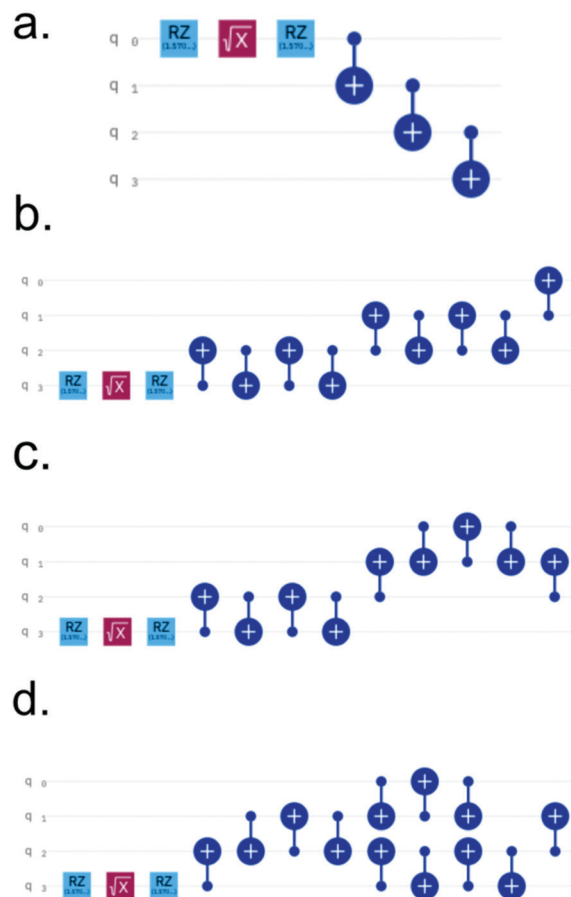

Fig. 3 (a) Transpiled circuits for the stair–step algorithm for 4-qubit cat states, and (b–d) three different transpiled circuits for the harpsichord algorithm for 4-qubit cat states, generated within a single job on manila.

slope for the harpsichord algorithm on melbourne ($m = 0.8055$, $R^2 = 0.9974$). Fewer gates are typically needed to implement the stair-step algorithm than the harpsichord algorithm. The value of S_{So} is lower for the stair-step algorithm than for the harpsichord algorithm in all but one of the cases.

We have also found differences in the outcomes depending on the connectivity of the qubits on the quantum computers. The two most common layouts on IBM's publicly accessible 5-qubit quantum computers are linear (santiago,[178] manila,[31] and athens[185]) with connections 0-1-2-3-4, and T-shaped (belem,[32] lima,[30] and quito[186]), with qubits 0-1-2 connected on the horizontal cross-bar of the T and qubits 1-3-4 connected on the vertical bar. The qubits on yorktown[184] have a more connected "bow-tie" layout. The qubit layout on melbourne[187] has two parallel rows connected linearly in each row, with paired connections from row to row; the two qubits at the opposite ends of the top row and the bottom row are connected only to the other qubits of that same row.

For the 5-qubit cat states, more gates are needed to implement the stair-step algorithm for a T-shaped layout than for a linear layout, because extra gates are needed to entangle q2 and q3 in the T-shape. The stair-step algorithm still requires fewer CNOT gates than the harpsicord algorithm, but the differences

Table 2 The Shannon entropy S_{So} of the distribution over measurement outcomes on santiago,[178] athens,[185] manila,[31] belem,[32] lima,[30] quito,[186] yorktown,[184] and melbourne[187] for cat states with the number n of entangled qubits between 2 and 5. Averages over 75 runs of 8192 shots each are shown. Results are listed separately for the stair-step algorithm and the harpsichord algorithm for $n = 3-5$. All of these computers have 5 qubits, except for melbourne which has 15 qubits

N	santiago	athens	manila	belem	lima	quito	yorktown	melbourne
2	1.24663	1.19388	1.35080	1.31211	1.25082	1.36915	1.63605	1.62569
Stair-step								
3	1.40940	1.42986	1.60570	1.62277	1.54037	1.67788	2.12485	2.30840
4	1.50907	1.60819	1.90407	2.09768	2.08562	1.97081	2.58539	2.79829
5	1.76001	1.87863	2.14523	2.67256	2.55860	2.46671	3.05493	3.64332
Harpsichord								
3	1.55625	1.53848	1.69420	1.85174	1.59762	1.74380	2.19417	2.36785
4	1.84393	1.96953	2.24983	2.35573	2.05140	2.23695	2.79926	3.52877
5	2.28568	2.38577	2.68380	2.78272	2.78139	2.76136	3.55477	4.25426
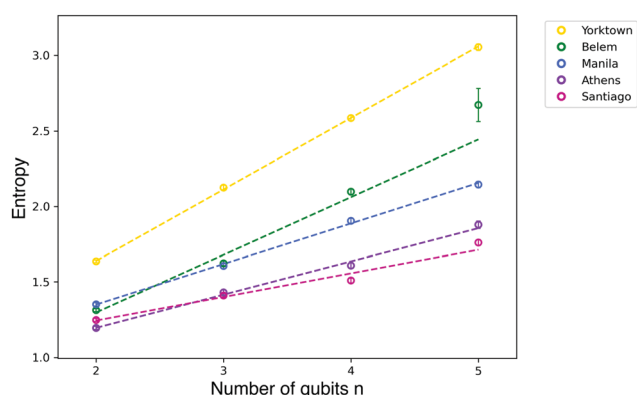
Fig. 4 The Shannon entropy S_{So} of the distribution over measurement outcomes for the stair-step algorithm, plotted as a function of the number of entangled qubits on the 5-qubit computers yorktown,[184] belem,[32] manila,[31] athens,[185] and santiago.[178]

between the S_{So} values for the two algorithms are less dramatic for the T-shaped layouts than for the linear layouts. The best pairing of the quantum algorithm with the qubit layout generally reduces the entropy of the measured outcomes and leads to better performance of the quantum computers on the current task.

Because the entanglement entropy has a direct connection to the thermodynamic entropy,[35,38,133] it is interesting to compare the entanglement entropy with the Shannon entropy S_{So} of the distribution over measurement outcomes. The relationship between the two depends on the quality of the cat states. If the cat states and measurements are fault-free, then the Shannon entropy S_{So} is identical to the entanglement entropy (*i.e.*, the von Neumann entropy of the reduced density matrices). Otherwise, S_{So} differs from the entanglement entropy. For example, the entanglement entropy of each of the qubits in the 3-qubit cat state in Fig. 1 is very close to one, while we have obtained an average Shannon entropy of the distribution over measurement outcomes for these 3-qubit cat states that is closer to 1.4.

The Shannon entropy S_{So} of an ideal state is not always equal to the entanglement entropy, however. For an ideal three-qubit W state, $(1/3)^{1/2} [|\alpha(1)\,\alpha(2)\,\beta(3)\rangle + |\alpha(1)\,\beta(2)\,\alpha(3)\rangle + |\beta(1)\,\alpha(2)\,\alpha(3)\rangle]$, $S_{So} = \log_2 3$, while the entanglement entropy is $\log_2 3 - 2/3$.

The n-qubit generalization of the W state contains n terms, with a different qubit in the β spin state in each of the terms and the remaining qubits all in the α spin state. For an ideal n-qubit W state $S_{So} = \log_2 n$, while the entanglement entropy is $\log_2 n - [(n-1)/n]\log_2(n-1)$.

IV. Model for the entropy as a function of the number of qubits

We have developed a simple model for S_{So} based on the probability a that an outcome of 0 will be observed when a qubit has been prepared in state $|0\rangle$ and the probability b that an outcome of 1 will be observed when a qubit has been prepared in state $|1\rangle$. When an n-qubit cat state is prepared, the probability $p(q, n-q)$ of obtaining a measurement outcome with q entries of 0 and $n-q$ entries of 1 is

$$p(q,\ n-q) = (1/2)C(n,\ q)[a^q(1-a)^{n-q} + (1-b)^q b^{n-q}], \quad (7)$$

where $C(n, q)$ denotes the number of combinations of n items taken q at a time. The Shannon entropy $S_{So}(n)$ of the distribution over measurement outcomes for an n-qubit cat state is therefore

$$S_{So}(n) = -\sum_{q=0}^{n} p(q, n-q) \log_2 [p(q, n-q)]. \quad (8)$$

In Fig. 6a and b, the entropy is plotted as a function of a and b, for various values of n. Fig. 6a shows S_{So} for a 4-qubit cat state, while Fig. 6b shows $S_{So}(n)$ for $n = 2, 5, 10,$ and 15, with the plots stacked on each other. In each case, the maximum Shannon entropy is $S_{So}(n) = n$, which is found when $a = b = 1/2$. It is apparent from the plots that the entropy is close to n over a range of values of (a, b), because the plots are almost flat near their maxima. This is especially evident in Fig. 6a. The range of values of (a, b) where $S_{So}(n)$ is close to n becomes narrower as n increases. The entropy $S_{So}(n) = 1$ when $a = b = 1$, which would yield a fault-free cat state. In an extreme case where $a = 0$ and $b = 1$ or $a = 1$ and $b = 0$, only one measurement outcome would be observed, giving $S_{So}(n) = 0$. The function $S_{So}(n)$ is symmetric in a and $1 - a$ and in b and $1 - b$. It is also symmetric with respect to interchange of a and b.

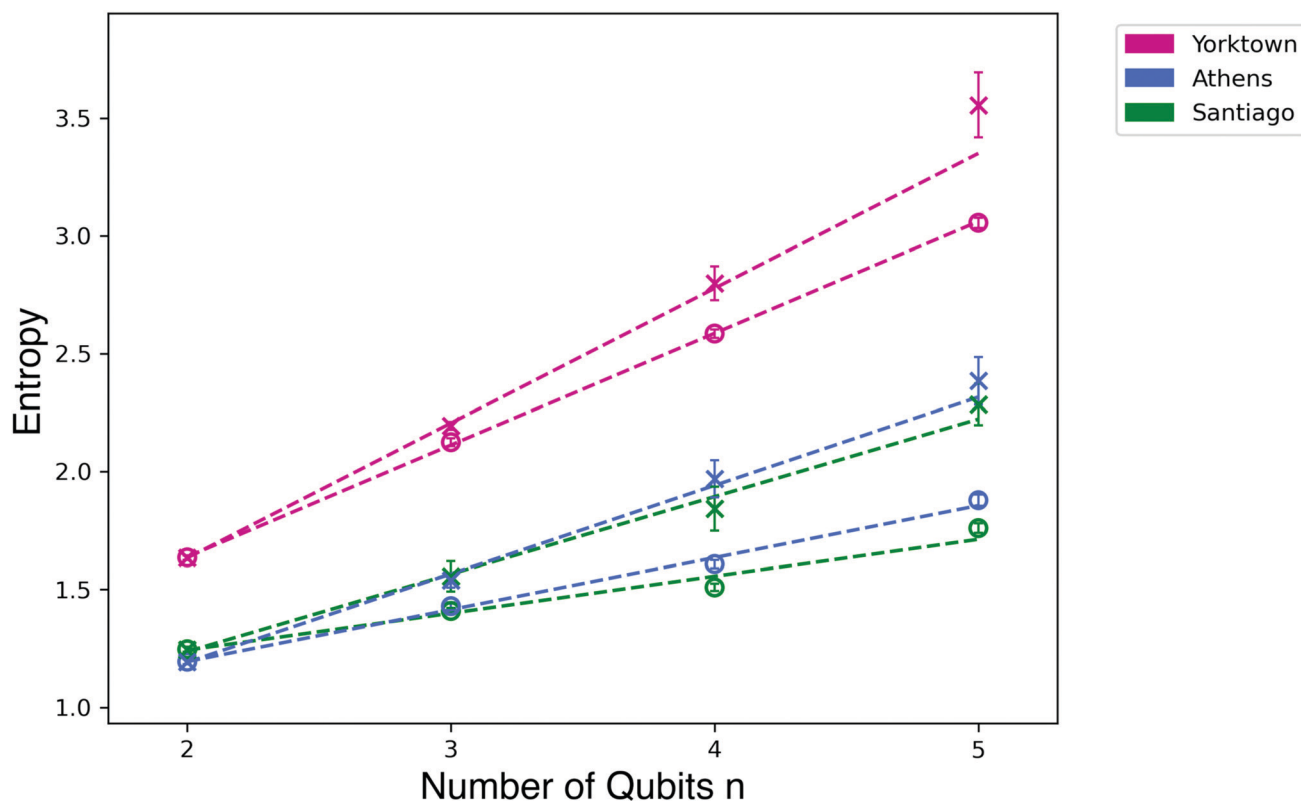This journal is © the Owner Societies 2022

Phys. Chem. Chem. Phys., 2022, **24**, 7666–7681 | **7673**

Fig. 5 Comparision of the Shannon entropies S_{So} for the two algorithms on IBMQ's yorktown,[184] athens,[185] and santaigo[178] computers. x: Harpsichord algorithm, o: stair-step algorithm. The error bars indicate one standard deviation from the average values of 75 runs.

Table 3 Slopes, intercepts, and R^2 values for the linear least-squares fits to S_{So} for santiago,[178] athens,[185] manila,[31] belem,[32] lima,[30] quito,[186] yorktown,[184] and melbourne.[187] The data have been weighted by the inverse of the variances of the entropies, based on 75 runs of 8192 shots each, on each computer. Results are shown for both the stair-step and harpsichord algorithms

	Stair-step algorithm			Harpsichord algorithm		
	Slope	Intercept	R^2	Slope	Intercept	R^2
santiago	0.1565	0.9303	0.9746	0.3285	0.5797	0.9917
athens	0.2204	0.7539	0.9956	0.3749	0.4421	0.9955
manila	0.2689	0.8115	0.9987	0.4216	0.5045	0.9882
belem	0.3823	0.5324	0.9831	0.5146	0.2837	0.9982
lima	0.3269	0.5866	0.9576	0.4625	0.3216	0.9765
quito	0.3106	0.7460	0.9936	0.3895	0.5869	0.9923
yorktown	0.4739	0.6908	0.9998	0.5720	0.4897	0.9976
melbourne	0.7315	0.0939	0.9881	0.8055	0.0170	0.9974

In the first version of this model, we used the average values of a and b for the qubits on each of the computers to find $S_{So}(n)$ as a function of n. The values for each qubit are tabulated by IBM and updated after the calibration runs on the computers. While it would be possible to develop a more detailed model based on the accuracy of producing states $|0\rangle$ and $|1\rangle$ on individual qubits, it would be necessary to track the specific qubits activated in each of the 75 circuits, after they have been transpiled. It would also be necessary to disaggregate the probabilities in eqn (7) by identifying the particular qubits in

states $|0\rangle$ and $|1\rangle$ since (for example) the probabilities of the outcomes 0 0 1, 0 1 0, and 1 0 0 would be distinct, rather than identical. Additionally, the specifics of the CNOT gates would need to be included in a more detailed model, along with a representation of the crosstalk between qubits and the effects of stray fields.

Our simple model suffices to account for the near linearity of the plots of $S_{So}(n)$ *versus* n, which is the principal objective of the model. As expected, the slopes are smaller when a and b are closer to one. As shown by comparison of entries in Tables 3 and 4, the slopes calculated with the average a and b values differ from the observed slopes for the stair-step algorithm; however, the slopes are correlated. In all but one case, the observed slopes are larger, probably due to additional error sources that are not included in the model with the average a and b values.

In a second version of the model, we have identified effective values a' and b' for each computer, by matching the modeled and observed slopes of S_{So} *versus* n to four figures. The values of a' and b' tend to be smaller than a and b. We have constrained a' and b', so that the ratio $a'/b' = a/b$ for each computer. Fits to the empirical and model results for S_{So} *vs.* n on the 5-qubit computers yorktown,[184] belem,[32] manila,[31] athens,[185] and santiago[178] are shown in Fig. 7. The model results for yorktown are in excellent agreement with the empirical results. We have examined the difference Δ between the intercept of the linear fit to the model for $S_{So}(n)$ and the intercept of the weighted linear
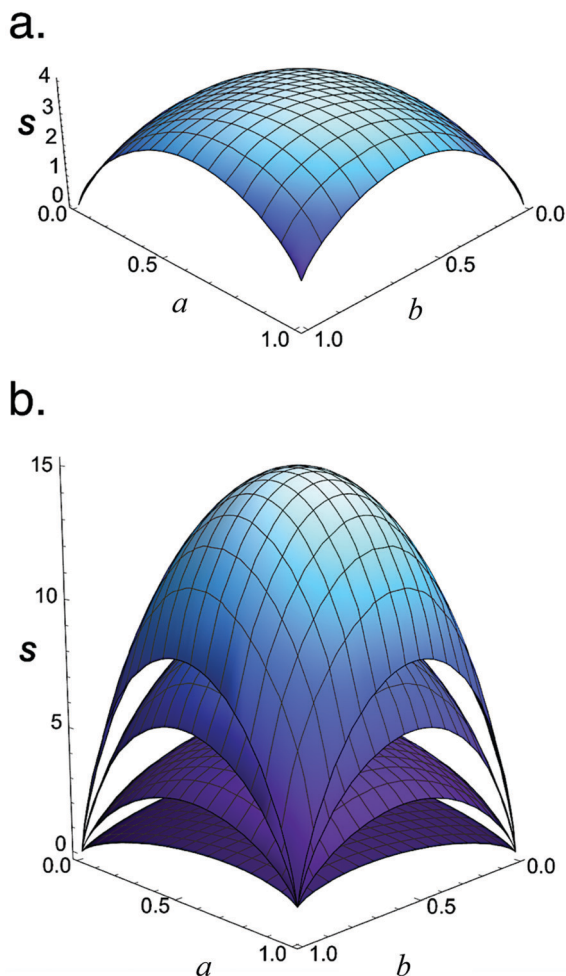
7674 | *Phys. Chem. Chem. Phys.*, 2022, **24**, 7666–7681

This journal is © the Owner Societies 2022

Fig. 6 Entropy S as a function of a and b, the accuracy of production and measurement of qubit states $|0\rangle$ and $|1\rangle$. (a) S for a 4-qubit cat state and (b) S for cat states with 2, 5, 10, and 15 qubits (stacked from bottom to top). A maximum value of the entropy equal to the number of qubits is found when $a = b = 0.5$.

least-squares fit to the empirical results for $S_{So}(n)$. For yorktown, Δ is only 0.0018, which accounts for the high quality of the fit with the model. For manila and athens, $S_{So}(n)$ from the quantum computer runs lies very nearly on a straight line. The discrepancies between the model and the quantum computer results are

mainly due to larger Δ values, 0.0569 on manila and 0.1544 on athens. The model fit for santiago is good, though not as good as for yorktown, primarily due to the slight deviation of $S_{So}(n)$ from a straight line. Still, the R^2 value for the stair-step algorithm on santiago is 0.9746. On quito and lima (not shown), the fit of the model is slightly better than on athens, but not as good as on santiago. For belem, the empirical averages for $S_{So}(n)$ are furthest from the model; belem has the largest Δ value of the 5-qubit computers, at 0.2464. On belem, the variance in the values of $S_{So}(n = 5)$ is more than one hundred times the variance in $S_{So}(n = 2)$, while for yorktown and santiago, the ratio of these variances is less than five.

Fig. 8 shows the comparison of the model and the weighted linear least-squares fit to the averages of $S_{So}(n)$ found with the stair-step and harpsichord algorithms on melbourne.[187] The standard deviation of $S_{So}(n)$ increases with n; the lower weight for the points with larger n causes those points to lie further from the straight-line fit. Even though Δ for melbourne is the largest we have found (at 0.4897), the model and the empirical results agree reasonably well, due to the comparatively large values of $S_{So}(n)$ in this case.

Extrapolating the linear fits obtained from the models based on (a, b) and (a', b') to obtain $S_{So}(n = 1)$ tends to yield larger values than those obtained by extrapolation of the linear fits of the empirical results to $S_{So}(n = 1)$. For an ideal single-qubit state $(1/2)^{1/2} (|0\rangle + |1\rangle)$, the entropy of the distribution over measurement outcomes should be equal to one. Values lower than one for the Shannon entropy $S_{So}(n = 1)$ reflect an imbalance between the probabilities of obtaining 0 or 1 for a qubit prepared in the state $(1/2)^{1/2} (|0\rangle + |1\rangle)$, with 0 usually being more common. Errors in the production and measurement of the cat states may cause the *extrapolated* empirical values of $S_{So}(n = 1)$ to exceed one.

Based on the fits with (a', b'), the extrapolated values of $S_{So}(n = 1)$ in the model range from 1.0952 on santiago[178] to 1.1665 on yorktown.[184] The extrapolated values of $S_{So}(n)$ for $n = 1$, based on the least-squares fit to the empirical results for the stair-step algorithm, cover a broader range from 0.8254 (on melbourne[187]) to 1.1647 on yorktown,[184] but the remaining results are clustered in the range from 0.9135 to 1.0868. For the harpsichord algorithm, extrapolations of $S_{So}(n)$ to $n = 1$ based on the empirical results typically give values smaller than one,

Table 4 Average values of the accuracy of single-qubit state production a and b (see text), and the slopes, intercepts, and R^2 values for linear least-squares fits to the entropy S_{So} as a function of the number of qubits. Values a' and b' were selected to reproduce the observed slopes of S_{So} from the stair-step algorithm to four figures. The slopes, intercepts and R^2 values for the fits with a' and b' are listed. The intercepts should be compared with the intercepts for S_{So} for the stair-step algorithm listed in Table 3

	a	b	Slope	Intercept	R^2	a'	b'	Slope	Intercept	R^2
santiago	0.9901	0.9795	0.1216	0.9574	0.9997	0.9848	0.9743	0.1565	0.9387	0.9976
athens	0.9792	0.9428	0.2563	0.9641	0.9996	0.9854	0.9488	0.2204	0.9083	0.9982
manila	0.9898	0.9682	0.1551	0.9439	0.9981	0.9704	0.9492	0.2689	0.8684	0.9977
belem	0.9874	0.9499	0.2103	0.9161	0.9983	0.9546	0.9183	0.3823	0.7788	0.9981
lima	0.9900	0.9589	0.1782	0.9347	0.9983	0.9633	0.9331	0.3269	0.8251	0.9979
quito	0.9896	0.9583	0.1814	0.9327	0.9983	0.9667	0.9361	0.3106	0.8384	0.9979
Yorktown	0.9591	0.9186	0.3964	0.7907	0.9981	0.9353	0.8958	0.4739	0.6926	0.9985
melbourne	0.9839	0.9298	0.8055	0.0170	0.9974	0.8329	0.7871	0.7315	0.5826	0.9995

This journal is © the Owner Societies 2022

Phys. Chem. Chem. Phys., 2022, **24**, 7666–7681 | **7675**
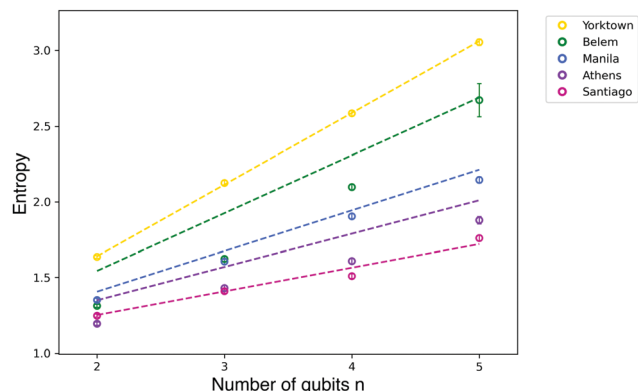
Fig. 7 Plot of $S_{So}(n)$ *vs. n* for the quantum computer outputs, compared with linear fits based on a' and b' (see text). Results obtained on yorktown,[184] belem,[32] manila,[31] athens,[185] and santiago.[178]
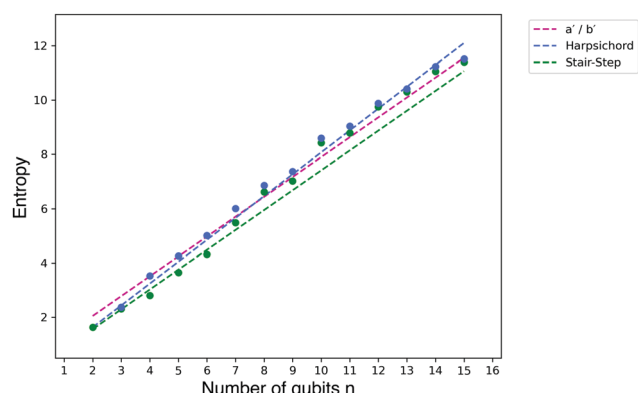

Fig. 8 Entropy S_{So} of the distribution over measurement outcomes for the model based on a' and b', compared with weighted linear least-squares fits of results obtained with the stair–step and harpsichord algorithms on melbourne.[187]

in the range from 0.7841 (on lima[30]) to 0.9261 (on manila[31]). Only yorktown[184] gives a value greater than one, at 1.0617.

V. Discussion and summary

Based on the results in this work, we suggest that the slope of a least-squares fit to S_{So}, the average Shannon entropy of the distribution over measurement outcomes for Schrödinger's cat states, provides a useful index of performance for noisy intermediate-scale quantum (NISQ) computers. The designation NISQ was introduced by Preskill.[188] The slope can be obtained quickly, and its values differentiate among computers that have identical quantum volumes. The quantum volume[148–151] indicates the suitability of a quantum computer for a much wider range of applications, since it is defined by considering square circuits and heavy outputs of at least 100 different circuits.[148] A circuit is square if the number of qubits is equal to the instruction depth. By definition, the heavy outputs are those whose probability exceeds the median output probability. The quantum volume is based on the largest square circuits for

which 2/3 or more of the outputs are heavy at the 97.5% confidence level. If the largest such square circuits have *n* qubits, then the quantum volume is 2^n (ref. 147). The more recent 5-qubit computers have a quantum volume of 32, which is the largest possible value for a 5-qubit device. Yet the performance of the computers in this group differs, and the slopes that we have found for $S_{So}(n)$ *versus n* indicate the differences.

Blume-Kohout and Young have suggested an alternative to the quantum volume, based on circuits with the depth and number of qubits uncoupled.[189] Another alternative based on a specific suite of application-oriented benchmarks has recently been suggested by Lubinksi *et al.*[190] We have explored a variant of the quantum volume that is specific to the cat-state algorithms. We identify the two outputs that should be observed for these states as the heavy outputs (either 0 for all qubits or 1 for all qubits). We have found the quantum volume as usual—but limited to the cat-state algorithm.

In Table 5, we illustrate the algorithm-specific quantum volume calculations by listing the percentages of the heavy outputs for 25 runs on lima[30] for various numbers of qubits, the averages for those 25 runs and for 75 runs, and the standard deviations. We have worked with the standard deviation of the percentage of heavy outputs in the individual runs, rather than the standard deviation of the mean, which is smaller. Thus our estimates of the algorithm-specific quantum volumes are conservative, but they are applicable to the likelihood of obtaining at least 2/3 heavy outputs in an individual run. For $n = 2$, 3, and 4, the value 2/3 lies 125.10, 84.75, and 10.22 standard deviations below the mean percentage of the heavy outputs, respectively; but for $n = 5$, 2/3 lies only 1.728 standard deviations below the mean percentage, so in this case, the quantum volume specific to the cat states is 16, which is larger than the quantum volume of 8 listed by IBM. (The *z* scores listed in Table 5 are based on all figures in the means and standard deviations, not just the rounded figures.)

We have compared the general-purpose quantum volumes V_g with the cat-state specific quantum volumes V_c for the stair-step algorithm on other quantum computers: V_c agrees with V_g at 32 for santiago,[178] athens,[185] and manila.[31] For belem[32] and quito,[186] V_c is 32, although V_g is 16. For yorktown[184] as for lima,[30] V_c is 16 for the stair-step algorithm, but V_g is 8. For melbourne,[187] V_c and V_g both equal 8. For the harpsichord circuits, the cat-state specific quantum volumes agree with the general-purpose quantum volumes on santiago, athens, and manila (at 32), and on belem and quito (at 16). The value of V_g is 8 for lima, yorktown, and melbourne, but the V_c values for the harpsichord circuits are 16, 8, and 4, respectively.

To summarize, we have evaluated the von Neumann entropies of *n*-qubit Schrödinger's cat states (for $n \leq 5$) by use of tomography on IBM's publicly accessible quantum computers. The von Neumann entropies exceed the expected value of zero for pure cat states, but error mitigation reduces the value of the von Neumann entropy. We have evaluated the entanglement entropies for individual qubits. As indicated by the reduced density matrices, the individual qubits are in mixed states with nearly equal populations of $|0\rangle$ and $|1\rangle$; the off-diagonal elements of the

7676 | *Phys. Chem. Chem. Phys.*, 2022, **24**, 7666–7681

This journal is © the Owner Societies 2022

Table 5 Percentages of heavy outputs for the cat states on lima.[30] Values are listed for 25 runs for qubit numbers 2 through 5. Cat states were constructed with the stair-step algorithm for $n = 3–5$. The averages and standard deviations of the 25 listed values are shown in the table, and the averages and standard deviations for a total of 75 runs are also shown. The z-score of 2/3 is listed at the end of the table

| | Percentages of heavy outputs | | | |
| | n | | | |
	2	3	4	5
Results of runs	95.813	90.967	84.802	68.396
	95.862	90.576	81.458	68.286
	95.410	91.199	81.799	74.133
	95.703	90.845	82.251	75.073
	95.544	90.771	81.604	69.128
	95.886	91.223	80.200	75.122
	95.801	90.710	79.358	68.762
	95.435	90.906	82.654	69.519
	95.837	91.223	80.298	74.780
	95.288	91.235	79.785	68.665
	95.581	90.515	83.740	72.119
	95.703	90.918	79.883	75.659
	95.581	91.284	80.762	74.194
	95.886	91.309	81.702	69.421
	95.654	91.162	82.422	72.192
	95.605	91.235	81.750	75.342
	96.021	91.089	80.444	72.681
	95.874	91.260	84.009	68.900
	95.850	90.820	80.420	69.373
	95.605	90.955	83.801	74.951
	95.923	90.991	81.714	69.348
	95.715	90.771	81.433	74.487
	95.813	91.016	84.155	67.798
	95.886	90.845	79.785	68.982
	95.862	91.455	81.409	74.817
Average of 25 runs	95.726	91.011	81.666	71.686
Standard deviation	0.182	0.244	1.527	2.897
Average of 75 runs	95.758	91.016	81.946	71.232
Standard deviation	0.233	0.287	1.495	2.642
z-Score for 2/3	125.10	84.75	10.22	1.728

density matrices are small. We have evaluated two forms of the Shannon entropy: S_{Sd} is derived from the diagonal elements of the density matrices, while S_{So} is obtained from the distribution over measurement outcomes for the projection of the "spins" along the z axis in the n-qubit cat states. For pure cat states, $S_{Sd}(n) = 1$, and for fault-free measurements on pure cat states, $S_{So}(n) = 1$, independent of n. On IBM's publicly accessible quantum computers, we have found that S_{So} actually increases nearly linearly with n. A simple two-variable model that employs the probabilities of observing outcomes 0 and 1 when the states $|0\rangle$ and $|1\rangle$ are initialized on a quantum computer accounts for the near linearity. The slope of $S_{So}(n)$ versus n provides a comparatively sensitive index of performance for NISQ computers.

Author contributions

Matthew Loucks, Scott Gilbert, Corbin Fleming-Dittenber, and Julia Egbert participated in the initial study of the Shannon entropy of the distribution of outcomes, directed by Katharine Hunt. This study provided the first evidence that S_{So} is nearly linear in the number of qubits. Nathan Jansen and Katharine Hunt developed the methodology and software for the investigation of the density matrices, the von Neumann entropy, and the Shannon entropy S_{Sd} derived from the diagonal elements of the density matrices. Nathan Jansen and Katharine Hunt extended the analysis of the Shannon entropy S_{So}; both are responsible for the data curation, formal analysis, validation, visualization, and writing. Katharine Hunt has been responsible for the project administration, supervision, and funding acquisition.

Conflicts of interest

Katharine Hunt is a member of the IBM Quantum Educators program, but this does not present a conflict of interest. The views expressed are those of the authors and do not reflect the official policy or position of IBM or the IBM Quantum team.

Acknowledgements

References

1 J. von Neumann, *Göttingen Nachrichten*, 1927, **1927**, 273–291.

2 C. E. Shannon, *Bell Syst. Tech. J.*, 1948, **27**, 379–423.

3 C. E. Shannon, *Bell Syst. Tech. J.*, 1948, **27**, 623–656.

4 D. Greenberger, M. Horne and A. Zeilinger, *Bell's Theorem, Quantum Theory, and Conceptions of the Universe*, Kluwer Academic, Dordrecht, 1989, p. 73.

5 IBM Q Experience is a trademark of International Business Machines Corporation, registered in many jurisdictions worldwide. See quantum-computing.ibm.com.

6 We have used quantum tomography of entangled states, as described in the IBM qiskit documentation qiskit.org/documentation/tutorials/noise/9_entanglement_verification.html. See also qiskit.org/documentation/tutorials/noise/8_tomography.html?highlight=error%20mitigation%20quantum%20tomography.

7 U. Fano, *Rev. Mod. Phys.*, 1957, **29**, 74–93.

8 R. G. Newton and B.-L. Young, *Ann. Phys.*, 1968, **49**, 393–402.

9 K. Vogel and H. Risken, *Phys. Rev. A: At., Mol., Opt. Phys.*, 1989, **40**, 2847–2849.

10 D. F. V. James, P. G. Kwiat, W. J. Munro and A. G. White, *Phys. Rev. A: At., Mol., Opt. Phys.*, 2001, **64**, 052312.

11 G. M. D'Ariano, L. Maccone and M. Paini, *J. Opt. B*, 2003, **5**, 77–84.

12 Y. X. Liu, L. F. Wei and F. Nori, *Europhys. Lett.*, 2004, **67**, 874–880.

13 C. F. Roos, G. P. T. Lancaster, M. Riebe, H. Häffner, W. Hänsel, S. Gulde, C. Becher, J. Eschner, F. Schmidt-Kaler and R. Blatt, *Phys. Rev. Lett.*, 2004, **92**, 220402.

14 V. N. Chernega, O. V. Man'ko, V. I. Man'ko, O. V. Pilyavets and V. G. Zborovskii, *J. Russ. Laser Res.*, 2006, **27**, 132–166.

15 M. Mirzaee, M. Rezaee and M. A. Jafarizadeh, *Int. J. Theor. Phys.*, 2007, **46**, 1471–1494.

16 O. J. Farias, C. L. Latune, S. P. Walborn, L. Davidovich and P. H. S. Ribeiro, *Science*, 2009, **324**, 1414–1417.

17 G. Toth, W. Wieczorek, D. Gross, R. Krischek, C. Schwemmer and H. Weinfurter, *Phys. Rev. Lett.*, 2010, **105**, 250403.

18 R. Blume-Kohout, *New J. Phys.*, 2010, **12**, 043034.

19 M. Cramer, M. B. Plenio, S. T. Flammia, R. Somma, D. Gross, S. D. Bartlett, O. Landon-Cardinal, D. Poulin and Y.-K. Liu, *Nat. Commun.*, 2010, **1**, 149.

20 V. I. Man'ko and I. V. Traskunov, *J. Russ. Laser Res.*, 2012, **33**, 269–275.

21 H. K. Ng and B. G. Englert, *Int. J. Quantum Information*, 2012, **10**, 1250038.

22 F. Huszar and N. M. T. Houlsby, *Phys. Rev. A: At., Mol., Opt. Phys.*, 2012, **85**, 052120.

23 T. Sugiyama, P. S. Turner and M. Murao, *Phys. Rev. Lett.*, 2013, **111**, 160406.

24 K. Bartkiewicz, K. Lemr and A. Miranowicz, *Phys. Rev. A: At., Mol., Opt. Phys.*, 2013, **88**, 052104.

25 G. I. Struchalin, I. A. Pogorelov, S. S. Straupe, K. V. Kravtsov, I. V. Radchenko and S. P. Kulik, *Phys. Rev. A*, 2016, **93**, 012103.

26 J. W. Shang, Z. Y. Zhang and H. K. Ng, *Phys. Rev. A*, 2017, **95**, 062336.

27 L. Pereira, L. Zambrano, J. Cortes-Vega, S. Niklitschek and A. Delgado, *Phys. Rev. A*, 2018, **98**, 012339.

28 R. Gupta, R. X. Xia, R. D. Levine and S. Kais, *PRX Quantum*, 2021, **2**, 010318.

29 K. Takeda, A. Noiri, T. Nakajima, J. Yoneda, T. Kobayashi and S. Tarucha, *Nat. Nanotechnol.*, 2021, **16**, 965–969.

30 ibmq_lima version 1.0.11, a 5-qubit IBM quantum computer with processor type Falcon r4 and a quantum volume of 8.

31 ibmq_manila, version 1.0.1, a 5-qubit IBM quantum computer with processor type Falcon r5.11L and a quantum volume of 32.

32 ibmq_belem, version 1.0.21, a 5-qubit IBM quantum computer with processor type Falcon r4T and a quantum volume of 16.

33 P. A. M. Dirac, *Math. Proc. Cambridge Philos. Soc.*, 1930, **26**, 376–385.

34 E. R. Davidson, *Reduced Density Matrices in Quantum Chemistry*, Academic Press, New York, 1976.

35 J. M. Deutsch, *Phys. Rev. A: At., Mol., Opt. Phys.*, 1991, **43**, 2046–2049.

36 H. Katsura, T. Hirano and Y. Hatsugai, *Phys. Rev. B: Condens. Matter Mater. Phys.*, 2007, **76**, 012401.

37 L. Z. Jiang, X. Y. Chen and T. Y. Ye, *Phys. Rev. A: At., Mol., Opt. Phys.*, 2011, **84**, 042308.

38 J. M. Deutsch, H. Li and A. Sharma, *Phys. Rev. E: Stat., Nonlinear, Soft Matter Phys.*, 2013, **87**, 042135.

39 M. Musz, M. Kuś and K. Życzkowski, *Phys. Rev. A: At., Mol., Opt. Phys.*, 2013, **87**, 022111.

40 C. Neill, P. Roushan, M. Fang, Y. Chen, M. Kolodrubetz, Z. Chen, A. Megrant, R. Barends, B. Campbell, B. Chiaro, A. Dunsworth, E. Jeffrey, J. Kelly, J. Mutus, P. J. H. O'Malley, C. Quintana, D. Sankt, A. Vainsencher, J. Wenner, T. C. White, A. Polkovnikov and J. M. Martinis, *Nat. Phys*, 2016, **12**, 1037–1041.

41 A. M. Kaufman, M. E. Tai, A. Lukin, M. Rispoli, R. Schittko, P. M. Preiss and M. Greiner, *Science*, 2016, **353**, 794–800.

42 J. Yuan, Y. Xing, L. Zhang and J. Wang, *Phys. Rev. B*, 2017, **95**, 155402.

43 K. Xu, J. J. Chen, Y. Zeng, Y. R. Zhang, C. Song, W. X. Liu, Q. J. Guo, P. F. Zhang, D. Xu, H. Deng, K. Q. Huang, H. Wang, X. B. Zhu, D. N. Zheng and H. Fan, *Phys. Rev. Lett.*, 2018, **120**, 050507.

44 S. Moitra and R. Sensarma, *Phys. Rev. B*, 2020, **102**, 184306.

45 J. Koch, T. M. Yu, J. Gambetta, A. A. Houck, D. I. Schuster, J. Majer, A. Blais, M. H. Devoret, S. M. Girvin and R. J. Schoelkopf, *Phys. Rev. A: At., Mol., Opt. Phys.*, 2007, **76**, 042319.

46 J. A. Schreier, A. A. Houck, J. Koch, D. I. Schuster, B. R. Johnson, J. M. Chow, J. M. Gambetta, J. Majer, L. Frunzio, M. H. Devoret, S. M. Girvin and R. J. Schoelkopf, *Phys. Rev. B: Condens. Matter Mater. Phys.*, 2008, **77**, 180502(R).

47 J. M. Gambetta, J. M. Chow and M. Steffen, *npj Quantum Information*, 2017, **3**, 2.

48 R. Barends, J. Kelly, A. Megrant, D. Sank, E. Jeffrey, Y. Chen, Y. Yin, B. Chiaro, J. Mutus, C. Neill, P. O'Malley, P. Roushan, J. Wenner, T. C. White, A. N. Cleland and J. M. Martinis, *Phys. Rev. Lett.*, 2013, **111**, 080502.

49 C. Rigetti, J. M. Gambetta, S. Poletto, B. L. T. Plourde, J. M. Chow, A. D. Córcoles, J. A. Smolin, S. T. Merkel, J. R. Rozen, G. A. Keefe, M. B. Rothwell, M. B. Ketchen and M. Steffen, *Phys. Rev. B: Condens. Matter Mater. Phys.*, 2012, **86**, 100506(R).

50 A. Ekert, P. M. Hayden and H. Inamori, *Coherent Matter Waves, Les Houches Summer School Session*, 2001, **72**, 663–701.

51 M. A. Nielsen and I. L. Chuang, *Quantum Computation and Quantum Information*, 10th anniversary edition, Cambridge University Press, Cambridge, UK, 2010.

52 Qiskit documentation at qiskit.org/documentation/stubs/qiskit.circuit.library.HGate.html.

53 Qiskit documentation at qiskit.org/documentation/stubs/qiskit.circuit.library.CXGate.html.

54 Qiskit documentation at qiskit.org/textbook/ch-gates/more-circuit-identities.html.

55 J. S. Bell, *Physics, Physique, Fizika*, 1964, **1**, 195–290.

7678 | *Phys. Chem. Chem. Phys.*, 2022, **24**, 7666–7681

This journal is © the Owner Societies 2022

56 J. S. Bell, *Speakable and Unspeakable in Quantum Mechanics*, Cambridge University Press, Cambridge, England, 2004.

57 J. Preskill, *Quantum Shannon Theory, Chapter 10 of lecture notes for PH219* (2018). http://theory.caltech.edu/∼preskill/ph219/chap10_6A.pdf.

58 M. Tiotsop, A. J. Fotue, G. K. Fautso, C. S. Kenfack, H. B. Fotsin and L. C. Fai, *Superlattices Microstruct.*, 2017, **103**, 70–77.

59 M. Tiotsop, G. K. Fautso, A. J. Fotue, H. B. Fotsin and L. C. Fai, *Indian J. Phys.*, 2020, **94**, 333–340.

60 A. J. Fotue, N. Issofa, M. Tiotsop, S. C. Kenfack, M. P. Tabue Djemmo, A. V. Wirngo, H. Fotsin and L. C. Fai, *Superlattices Microstruct.*, 2016, **90**, 20–29.

61 M. Hô, H. L. Schmider, D. F. Weaver, V. H. Smith, Jr., R. P. Sagar and R. O. Esquivel, *Int. J. Quantum Chem.*, 2000, **77**, 376–382.

62 S. Bera, S. K. Haldar, B. Chakrabarti, A. Trombettoni and V. K. B. Kota, *Eur. Phys. J. D*, 2020, **74**, 73.

63 A. Rényi, *Proceedings of the Fourth Berkeley Symposium on Mathematics, Statistics, and Probability*, 1961, pp. 547–561.

64 I. Csiszár, *IEEE Trans. Information Theory*, 1995, **41**, 26–34.

65 V. N. Chernega and V. I. Man'ko, *J. Russ. Laser Res.*, 2008, **29**, 505–519.

66 F. Franchini, A. R. Its and V. E. Korepiin, *J. Phys. A: Math. and Theor.*, 2008, **41**, 025302.

67 A. R. Its and V. E. Korepin, *Theor. Math. Phys.*, 2010, **164**, 1136–1139.

68 J. Zhang, Y. Zhang and C.-S. Yu, *Quantum Inf. Process.*, 2015, **14**, 2239–2253.

69 S. Johri, D. S. Steiger and M. Troyer, *Phys. Rev. B*, 2017, **96**, 195136.

70 N. M. Linke, S. Johri, C. Figgatt, K. A. Landsman, A. Y. Matsuura and C. Monroe, *Phys. Rev. A*, 2018, **98**, 052334.

71 O. Olendski, *Int. J. Quantum Chem.*, 2020, **120**, e26220.

72 T. Brydges, A. Elben, P. Jurcevic, B. Vermersch, C. Maier, B. P. Lanyon, P. Zoller, R. Blatt and C. F. Roos, *Science*, 2019, **364**, 260–263.

73 A. Wehrl, *Rev. Mod. Phys.*, 1978, **50**, 221–260.

74 A. Wehrl, *Rep. Math. Phys.*, 1977, **12**, 385–394.

75 A. Miranowicz, J. Bajer, M. R. B. Wahiddin and N. Imoto, *J. Phys. A: Math. Gen.*, 2001, **34**, 3887–3896.

76 C. Tsallis, *J. Stat. Phys.*, 1988, **52**, 479–487.

77 C. Tsallis, S. Lloyd and M. Baranger, *Phys. Rev. A: At., Mol., Opt. Phys.*, 2001, **63**, 042104.

78 A. S. Nayak, Sudha, A. K. Rajagopal and A. R. Usha Devi, *Phys. A*, 2016, **443**, 286–295.

79 J. S. Kim, *Phys. Rev. A: At., Mol., Opt. Phys.*, 2010, **81**, 062328.

80 R. Khordad and H. R. R. Sedehi, *Superlattices Microstruct.*, 2017, **101**, 559–566.

81 M. Tiotsop, A. J. Fotue, H. B. Fotsin and L. C. Fai, *Superlattices Microstruct.*, 2017, **105**, 163–171.

82 Č. Brukner and A. Zeilinger, *Phys. Rev. Lett.*, 1999, **83**, 3354–3357.

83 Č. Brukner and A. Zeilinger, *Phys. Rev. A: At., Mol., Opt. Phys.*, 2001, **63**, 022113.

84 S. Sakamoto and Y. Tanimura, *J. Chem. Phys.*, 2020, **153**, 234107.

85 L. Boltzmann, *Sitzungsberichte Akademie der Wissenschaften*, 1872, **66**, 275–370.

86 S. J. Freedman and J. F. Clauser, *Phys. Rev. Lett.*, 1972, **28**, 938–941.

87 E. S. Fry and R. C. Thompson, *Phys. Rev. Lett.*, 1976, **37**, 465–468.

88 A. Aspect, P. Grangier and G. Roger, *Phys. Rev. Lett.*, 1981, **47**, 460–463.

89 A. Aspect, P. Grangier and G. Roger, *Phys. Rev. Lett.*, 1982, **49**, 91–94.

90 A. Aspect, J. Dalibard and G. Roger, *Phys. Rev. Lett.*, 1982, **49**, 1804–1807.

91 J. F. Clauser, M. A. Horne, A. Shimony and R. A. Holt, *Phys. Rev. Lett.*, 1969, **23**, 880–884.

92 A. Garg and N. D. Mermin, *Phys. Rev. D*, 1987, **35**, 3831–3835.

93 P. H. Eberhard, *Phys. Rev. A: At., Mol., Opt. Phys.*, 1993, **47**, R747–R750.

94 J. Barrett, D. Collins, L. Hardy, A. Kent and S. Popescu, *Phys. Rev. A: At., Mol., Opt. Phys.*, 2002, **66**, 042111.

95 M. Giustina, A. Mech, S. Ramelow, B. Wittmann, J. Kofler, J. Beyer, A. Lita, B. Calkins, T. Gerrits, S. Nam, R. Ursin and A. Zeilinger, *Nature*, 2013, **497**, 227–230.

96 B. G. Christensen, K. T. McCusker, J. B. Altepeter, B. Calkins, T. Gerrits, A. E. Lita, A. Miller, L. K. Shalm, Y. Zhang, S. W. Nam, N. Brunner, C. C. W. Lim, N. Gisin and P. G. Kwiat, *Phys. Rev. Lett.*, 2013, **111**, 130406.

97 J. A. Larsson, M. Giustina, J. Kofler, B. Wittmann, R. Ursin and S. Ramelow, *Phys. Rev. A: At., Mol., Opt. Phys.*, 2014, **90**, 032107.

98 K. F. Pal and T. Vertesi, *Phys. Rev. A: At., Mol., Opt. Phys.*, 2015, **92**, 022103.

99 M.-H. Li, C. Wu, Y. Zhang, W.-Z. Liu, B. Bai, Y. Liu, W. Zhang, Q. Zhao, H. Li, Z. Wang, L. You, W. J. Munro, J. Yin, J. Zhang, C.-Z. Peng, X. Ma, Q. Zhang, J. Fan and J.-W. Pan, *Phys. Rev. Lett.*, 2018, **121**, 080404.

100 K. Sen, S. Das and U. Sen, *Phys. Rev. A*, 2019, **100**, 062333.

101 G. Weihs, T. Jennewein, C. Simon, H. Weinfurter and A. Zeilinger, *Phys. Rev. Lett.*, 1998, **81**, 5039–5043.

102 J. Handsteiner, A. S. Friedman, D. Rauch, J. Gallicchio, B. Liu, H. Hosp, J. Kofler, D. Bricher, M. Fink, C. Leung, A. Mark, H. T. Nguyen, I. Sanders, F. Steinlechner, R. Ursin, S. Wengerowsky, A. H. Guth, D. I. Kaiser, T. Scheidl and A. Zeilinger, *Phys. Rev. Lett.*, 2017, **118**, 060401.

103 W. Tittel, J. Brendel, H. Zbinden and N. Gisin, *Phys. Rev. Lett.*, 1998, **81**, 3563–3566.

104 A. Fedrizzi, R. Ursin, T. Herbst, M. Nespoli, R. Prevedel, T. Scheidl, F. Teifenbacher, T. Jennewein and A. Zeilinger, *Nat. Phys.*, 2009, **5**, 389–392.

105 For a review, see N. Brunner, D. Cavalcanti, S. Pironio, V. Scarani and S. Wehner, *Rev. Mod. Phys.*, 2014, **86**, 419–478 and 839.

106 N. D. Mermin, *Phys. Rev. Lett.*, 1990, **65**, 1838–1840.

107 D. Alsina and J. I. Latorre, *Phys. Rev. A*, 2016, **94**, 012314.

108 A. J. Leggett and A. Garg, *Phys. Rev. Lett.*, 1985, **54**, 857–860.

109 E. Huffman and A. Mizel, *Phys. Rev. A*, 2017, **95**, 032131.

110 M. Ansmann, H. Wang, R. C. Bialczak, M. Hofheinz, E. Lucero, M. Neeley, A. D. O'Connell, D. Sank, M. Weides, J. Wenner, A. N. Cleland and J. M. Martinis, *Nature*, 2009, **461**, 504–506.

111 I. Hamamura, *Phys. Lett. A*, 2018, **382**, 2573–2577.

112 D. Z. Wang, A. Q. Gauthier, A. E. Siegmund and K. L. C. Hunt, *Phys. Chem. Chem. Phys.*, 2021, **23**, 6370–6387.

113 M. Sisodia, *Quantum Inf. Process.*, 2020, **19**, 215.

114 M. B. Pozzobom and J. Maziero, *Quantum Inf. Process.*, 2019, **18**, 142.

115 N. J. Cerf and C. Adami, *Phys. Rev. A: At., Mol., Opt. Phys.*, 1997, **55**, 3371–3374.

116 P.-Y. Chang, S.-K. Chu and C.-T. Ma, *Int. J. Modern Phys. A*, 2019, **34**, 1950032.

117 A. Elben, R. Kueng, H.-Y. Huang, R. van Bijnen, C. Kokail, M. Dalmonte, P. Calabrese, B. Kraus, J. Preskill, P. Zoller and B. Vermersch, *Phys. Rev. Lett.*, 2020, **125**, 200501.

118 J.-W. Pan, D. Bouwmeester, M. Daniell, H. Weinfurter and A. Zeilinger, *Nature*, 2000, **403**, 515–519.

119 J. Lavoie, R. Kaltenbaek and K. Resch, *New J. Phys.*, 2009, **11**, 073051.

120 D. Leibfried, E. Knill, S. Seidelin, J. Britton, R. B. Blakestead, J. Chiaverini, D. B. Hume, W. M. Itano, J. D. Jost, C. Langer, R. Ozeri, R. Reichle and D. J. Wineland, *Nature*, 2005, **438**, 639–642.

121 K. X. Wei, I. Lauer, S. Srinivasan, N. Sundaresan, D. T. McClure, D. Toyli, D. C. McKay, J. M. Gambetta and S. Sheldon, *Phys. Rev. A*, 2020, **101**, 032343.

122 G. J. Mooney, G. A. L. White, C. D. Hill and L. C. L. Hollenberg, *J. Phys. Commun.*, 2021, **5**, 095004.

123 ibmq_montreal, version 1.11.0, a 27-qubit IBM quantum computer with processor type Falcon r4 and a quantum volume of 128.

124 G. J. Mooney, G. A. L. White, C. D. Hill and L. C. L. Hollenberg, *Adv. Quantum Technol.*, 2021, **4**, 2100061.

125 ibmq_rochester, a 53-qubit IBM quantum computer, now retired.

126 ibmq_manhattan, a 65-qubit IBM quantum computer with processor type Hummingbird r2 and quantum volume of 32, now retired.

127 L. M. Sager, S. E. Smart and D. A. Mazziotti, *Phys. Rev. Res.*, 2020, **2**, 043205.

128 Y. J. Zhao, R. Zhang, W. L. Chen, X. B. Wang and J. Z. Hu, *NPJ Quantum Information*, 2021, **7**, 24.

129 W. Dür, G. Vidal and J. I. Cirac, *Phys. Rev. A: At., Mol., Opt. Phys.*, 2000, **62**, 062314.

130 M. Eibl, N. Kiesel, M. Bourennane, C. Kurtsiefer and H. Weinfurter, *Phys. Rev. Lett.*, 2004, **92**, 077901.

131 H. Häffner, W. Hänsel, C. F. Roos, J. Benhelm, D. Chek-al-kar, M. Chwalla, T. Körber, U. D. Rapol, M. Riebe, P. O. Schmidt, C. Becher, O. Gühne, W. Dür and R. Blatt, *Nature*, 2005, **438**, 643–646.

132 A. Omran, H. Levine, A. Keesling, G. Semeghini, T. T. Wang, S. Ebadi, H. Bernien, A. S. Zibrov, H. Pichler, S. Choi, J. Cui, M. Rossignolo, P. Rembold, S. Montangero, T. Calarco, M. Endres, M. Greiner, V. Vuletić and M. D. Lukin, *Science*, 2019, **365**, 570–574.

133 J. M. Deutsch, *Rep. Prog. Phys.*, 2018, **81**, 082001.

134 R. Islam, R. Ma, P. M. Preiss, M. E. Tai, A. Lukin, M. Rispoli and M. Greiner, *Nature*, 2015, **528**, 77–83.

135 D. Bluvstein, A. Omran, H. Levine, A. Keesling, G. Semeghini, S. Ebadi, T. T. Wang, A. A. Michailidis, N. Maskara, W. W. Ho, S. Choi, M. Serbyn, M. Greiner, V. Vuletic and M. D. Lukin, *Science*, 2021, **371**, 1355–1359.

136 K. Xu, J.-J. Chen, Y. Zeng, Y.-R. Zhang, C. Song, W. Liu, Q. Guo, P. Zhang, D. Xu, H. Deng, K. Huang, H. Wang, X. Zhu, D. Zheng and H. Fan, *Phys. Rev. Lett.*, 2018, **120**, 050507.

137 N. Wu and P. Yang, *Phys. Rev. B*, 2021, **103**, 174428.

138 G. Parez, R. Bonsignori and P. Calabrese, *J. Stat. Mech.*, 2021, **2021**, 093102.

139 A. Lukin, M. Rispoli, R. Schittko, M. E. Tai, A. M. Kaufman, S. Choi, V. Khemani, J. Leonard and M. Greiner, *Science*, 2019, **364**, 256–260.

140 X. L. Deng, G. Masella, G. Pupillo and L. Santos, *Phys. Rev. Lett.*, 2020, **125**, 010401.

141 D. Deutsch, *Phys. Rev. Lett.*, 1983, **50**, 631–633.

142 P. Jizba, J. A. Dunningham and J. Joo, *Ann. Phys.*, 2015, **355**, 87–114.

143 V. Majernik and T. Opatrný, *J. Phys. A: Math. Gen.*, 1996, **29**, 2187–2197.

144 Z. Chen, Z. Ma, Y. Xiao and S.-M. Fei, *Phys. Rev. A*, 2018, **98**, 042305.

145 I. Veeren and F. de Melo, *Phys. Rev. A*, 2020, **102**, 022205.

146 B. Bergh and M. Garttner, *Phys. Rev. A*, 2021, **103**, 052412.

147 B. Bergh and M. Garttner, *Phys. Rev. Lett.*, 2021, **126**, 190503.

148 A. W. Cross, L. S. Bishop, S. Sheldon, P. D. Nation and J. M. Gambetta, *Phys. Rev. A*, 2019, **100**, 032328.

149 N. Moll, P. Barkoutsos, L. S. Bishop, J. M. Chow, A. Cross, D. J. Egger, S. Filipp, A. Fuhrer, J. M. Gambetta, M. Ganzhorn, A. Kandala, A. Mezzacapo, P. Müller, W. Riess, G. Salis, J. Smolin, I. Tavernelli and K. Temme, *Quantum. Sci. Technol.*, 2018, **3**, 030503.

150 P. Jurcevic, A. Javadi-Abhari, L. S. Bishop, I. Lauer, D. F. Bogorin, M. Brink, L. Capelluto, O. Günlük, T. Itoko, N. Kanazawa, A. Kandala, G. A. Keefe, K. Krsulich, W. Landers, E. P. Lewandowski, D. T. McClure, G. Nannicini, A. Narasgond, H. M. Nayfeh, E. Pritchett, M. B. Rothwell, S. Srinivasan, N. Sundaresan, C. Wang, K. X. Wei, C. J. Wood, J.-B. Yau, E. J. Zhang, O. E. Dial, J. M. Chow and J. M. Gambetta, *Quantum. Sci. Technol.*, 2021, **6**, 025020.

151 J. M. Pino, J. M. Dreiling, C. Figgatt, J. P. Gaebler, S. A. Moses, M. S. Allman, C. H. Baldwin, M. Foss-Feig, D. Hayes, K. Mayer, C. Ryan-Anderson and B. Neyenhuis, *Nature*, 2021, **592**, 209–213.

152 The Class BConfig is part of IBM qiskit in the IBM Quantum Experience, as described at qiskit.org/documen tation/stubs/qiskit.ignis.verification.BConfig.html, retrieved during 10/2021. The documentation in ref. 153,

7680 | *Phys. Chem. Chem. Phys.*, 2022, **24**, 7666–7681

This journal is © the Owner Societies 2022

155-157, 163, 176, and 177 has also been retrieved during 10/2021.

153 Documentation for state_tomography_circuits in qiskit is provided at qiskit.org/documentation/stubs/qiskit.ignis.verification.state_tomography_circuits.html and qiskit.org/documentation/_modules/qiskit/ignis/verification/tomography/basis/circuits.html.

154 J. Cotler and F. Wilczek, *Phys. Rev. Lett.*, 2020, **124**, 100401.

155 The Class StateTomographyFitter in qiskit is described at qiskit.org/documentation/stubs/qiskit.ignis.verification.StateTomographyFitter.html.

156 The code fit is described at qiskit.org/documentation/stubs/qiskit.ignis.verification.StateTomographyFitter.fit.html.

157 The source code for state_fitter is available at qiskit.org/documentation/_modules/qiskit/ignis/verification/tomography/fitters/state_fitter.html.

158 Z. Hradil, *Phys. Rev. A: At., Mol., Opt. Phys.*, 1997, **55**, R1561–R1564.

159 K. Banasek, G. M. D'Ariano, M. G. A. Paris and M. F. Sacchi, *Phys. Rev. A: At., Mol., Opt. Phys.*, 2000, **61**, 010304.

160 Z. Hradil, J. Summhammer, G. Badurek and H. Rauch, *Phys. Rev. A: At., Mol., Opt. Phys.*, 2000, **62**, 014101.

161 J. Fiurasek and Z. Hradil, *Phys. Rev. A: At., Mol., Opt. Phys.*, 2001, **63**, 020101.

162 J. Smolin, J. M. Gambetta and G. Smith, *Phys. Rev. Lett.*, 2012, **108**, 070502.

163 Additional documentation of the CVPXY method can be found at www.cvxpy.org, (described as CVXPY "for everyone"), at www.cvxpy.org/tutorial/advanced/index/html, and at www.cvxpy.org/tutorial/advanced/index/html#solve-methods-options.

164 R. Blume-Kohout, *Phys. Rev. Lett.*, 2010, **105**, 200504.

165 Q. Yin, G.-Y. Xiang, C.-F. Li and G. C. Guo, *Chin. Phys. Lett.*, 2017, **34**, 030301.

166 T. Sagawa and M. Ueda, *Phys. Rev. A: At., Mol., Opt. Phys.*, 2008, **77**, 012313.

167 R. Derka, V. Bužek and A. K. Ekert, *Phys. Rev. Lett.*, 1998, **80**, 1571–1575.

168 E. Bagan, A. Monras and R. Munoz-Tapia, *Phys. Rev. A: At., Mol., Opt. Phys.*, 2005, **71**, 062318.

169 R. Blume-Kohout, *New J. Phys.*, 2010, **12**, 043034.

170 R. Schmied, *J. Modern Optics*, 2016, **63**, 1744–1758.

171 R. Gupta, R. D. Levine and S. Kais, *J. Phys. Chem. A*, 2021, **125**, 7588–7595.

172 P. E. Jupp, P. T. Kim, J.-Y. Koo and A. Pasieka, *J. Royal Stat. Soc. Series C*, 2012, **61**, 753–763.

173 D. Gross, Y. K. Liu, S. Flammia, S. Becker and J. Eisert, *Phys. Rev. Lett.*, 2010, **105**, 150401.

174 G. Tóth, W. Wieczorek, D. Gross, R. Krischek, C. Schwemmer and H. Weinfurter, *Phys. Rev. Lett.*, 2010, **105**, 250403.

175 T. Moroder, P. Hyllus, G. Z. Tóth, C. Schwemmer, A. Niggebaum, S. Gaile, O. Gühne and H. Weinfurter, *New J. Phys.*, 2012, **14**, 105001.

176 qiskit.org/documentation/stubs/qiskit.quantum_info.state_fidelity.html.

177 The Class CompleteMeasFitter is described at the website qiskit.org/documentation/stubs/qiskit.ignis.mitigation.CompleteMeasFitter.html. Source code for the measurement correction fitters can be found at qiskit.org/documentation/_modules/qiskit/ignis/mitigation/measurement/fitters.html#CompleteMeasFitter.add_data. See also qiskit.org/documentation/stubs/qiskit.ignis.mitigation.CompleteMeasFitter.html, and qiskit.org/documentation/stubs/qiskit.ignis.mitigation/complete_meas_cal.html. A description of meas_calibs is found at learn.qiskit.org/course/quantum-hardware/measurement-error-mitigation.

178 ibmq_santiago, version 1.3.22, a 5-qubit IBM quantum computer with processor type Falcon r4 and a quantum volume of 32.

179 S. Chatterjee and N. Makri, *Phys. Chem. Chem. Phys.*, 2021, **23**, 5113–5124.

180 S. Chatterjee and N. Makri, *Phys. Chem. Chem. Phys.*, 2021, **23**, 5125–5133.

181 J. A. Anaya-Contreras, H. M. Moya-Cessa and A. Zúñiga-Segundo, *Entropy*, 2019, **21**, 49.

182 ibmq_jakarta, version 1.0.21, a 7-qubit IBM quantum computer with processor type Falcon r5.11H, and a quantum volume of 16.

183 simulator_statevector, current version 0.1.547, a 32-qubit Schrödinger wavefunction simulator, accessed through the IBM Quantum Experience.

184 ibmq_yorktown, a 5-qubit IBM quantum computer, with connections (q0, q1), (q0, q2), (q1, q2), (q2, q3), (q2, q4), and (q3,q4), now retired.

185 ibmq_athens, version 1.3.19, a 5-qubit IBM quantum computer with processor type Falcon r4 and a quantum volume of 32, now retired.

186 ibmq_quito, version 1.1.2, a 5-qubit IBM quantum computer with processor type Falcon r4 and a quantum volume of 16.

187 ibmq_16_melbourne, version 2.3.24, a 15-qubit IBM quantum computer with processor type Canary r1.1 and a quantum volume of 8, now retired.

188 J. Preskill, *Quantum*, 2018, **2**, 79.

189 R. Blume-Kohout and K. Young, *Quantum*, 2020, **4**, 362.

190 T. Lubinski, S. Johri, P. Varosy, J. Coleman, L. Zhao, J. Necaise, C. H. Baldwin, K. Mayer and T. Proctor, Quantum Economic Development Consortium (QED-C) collaboration, arXiv 2110.03137, 7 Oct. 2021.

This journal is © the Owner Societies 2022

Phys. Chem. Chem. Phys., 2022, **24**, 7666–7681 | 7681